

# Adaptive aggregation of Monte Carlo augmented decomposed filters for efficient group-equivariant convolutional neural network

Wenzhao Zhao, Barbara D. Wichtmann, Steffen Albert, Angelika Maurer, Frank G. Zöllner and Jürgen Hesser

**Abstract**—Group-equivariant convolutional neural networks (G-CNN) heavily rely on parameter sharing to increase CNN’s data efficiency and performance. However, the parameter-sharing strategy greatly increases the computational burden for each added parameter, which hampers its application to deep neural network models. In this paper, we address these problems by proposing a non-parameter-sharing approach for group equivariant neural networks. The proposed methods adaptively aggregate a diverse range of filters by a weighted sum of stochastically augmented decomposed filters. We give theoretical proof about how the group equivariance can be achieved by our methods. Our method applies to both continuous and discrete groups, where the augmentation is implemented using Monte Carlo sampling and bootstrap resampling, respectively. Our methods also serve as an efficient extension of standard CNN. The experiments show that our method outperforms parameter-sharing group equivariant networks and enhances the performance of standard CNNs in image classification and denoising tasks, by using suitable filter bases to build efficient lightweight networks. The code will be available at [https://github.com/ZhaoWenzhao/MCG\\_CNN](https://github.com/ZhaoWenzhao/MCG_CNN).

**Index Terms**—Group equivariance, non-parameter-sharing, convolutional neural network, Monte Carlo sampling, filter decomposition.

## I. INTRODUCTION

**E**QUIVARIANCE or invariance under some transformation of input is a desired characteristic for many applications including computer vision tasks such as image classification and image denoising. This is due to the widespread existence of transformations such as affine transformations in natural images as shown in Fig. 1. For image classification, one may expect the classification algorithms to recognize the objects in the image regardless of any affine transformation, which is called “invariance”. For image denoising, we expect the denoiser to process transformed input images and to output a corresponding transformed outputs, which is called “equivariance”. Invariance can be considered a special case of “equivariance”. We see that an affine equivariant



Fig. 1. An example of affine transformation in real life. The image is from the CBS432 [4] dataset. As shown in the white rectangular box, the horizontal lines of bricks undergo a shear transform along the vertical direction.

deep learning model can have a good generalization and robustness against the affine transformation of the input image data. The deep learning methods that boost equivariance can therefore improve data efficiency of deep learning. To achieve equivariant deep learning, researchers generally adopt two different approaches: data augmentation [1], [2], and group-equivariant network architectures [3]. Data augmentation is an efficient and popular method for enhancing a given model’s group equivariance. However, there is no guarantee for group equivariance with respect to unseen data.

Group equivariant neural networks are another way to enhance group equivariant deep learning by focusing on the neural network’s architecture itself. Convolutional neural networks (CNNs), one of the most widespread deep neural network architectures in computer vision, shows a desirable property of translation equivariance due to its “sliding window” strategy inspired by human vision [5], [6]. In recent years, a sheer amount of publications have emerged aiming at developing and applying more advanced group equivariant CNNs to improve CNN’s sample efficiency and generalizability [7]–[9]. The concept of group equivariant CNN (G-CNN) was first proposed by Cohen and Welling in [10], which exploited a higher degree of weight sharing by increasing the number of convolutional channels with the periodical rotation of the same convolutional kernel. This idea was further extended in [11] by introducing steerable filters which decomposed the convolutional kernel with an orthogonal basis of roto-reflection groups.

Following the work of rotation equivariant CNN, in recent years, there have been a lot of studies based on filter decomposition for exploring scale equivariant CNN [12]–[15],

Wenzhao Zhao is with Interdisciplinary Center for Scientific Computing, Mannheim Institute for Intelligent Systems in Medicine, Medical Faculty Mannheim, Heidelberg University. Barbara D. Wichtmann and Angelika Maurer are with Department of Diagnostic and Interventional Radiology, University Hospital Bonn. Steffen Albert and Frank G. Zöllner are with Computer Assisted Clinical Medicine, Mannheim Institute for Intelligent Systems in Medicine, Medical Faculty Mannheim, Heidelberg University. Jürgen Hesser is with Interdisciplinary Center for Scientific Computing, Central Institute for Computer Engineering, CSZ Heidelberg Center for Model-Based AI, Data Analysis and Modeling in Medicine, Mannheim Institute for Intelligent Systems in Medicine, Medical Faculty Mannheim, Heidelberg University. E-mail: wenzhao.zhao@medma.uni-heidelberg.de.

Manuscript received April 19, 2021; revised August 16, 2021.

and scale-rotation equivariant CNN [8], [16]. Attention mechanisms have been introduced in [8], [17] to help better identify optimal filter banks and boost equivariance performance. The idea of group equivariance has also been introduced to transformer networks to improve the transformer’s data efficiency. Apart from filter decomposition, more recently, the feature alignment has also proven to be helpful for improving CNN’s group equivariance against affine image transforms [18].

The existing works for filter-decomposition-based group equivariant CNN all require increasing channel numbers to increase parameter-sharing degree. This is because the existing works are based on group convolution [3] [19] and performing group convolution needs lifting or mapping the image data to the transformation group space, where additional dimensions are introduced and the integration or average along the additional dimensions is handled by the same learnable parameters (causing a higher parameter-sharing degree). This integration along the additional dimensions brings in a heavy computational burden [7] and it causes an imbalance between the number of computational operations and the number of learnable parameters, which hence hampers their practical application to complex neural network architectures. Due to the computational burden needed for considering one kind of transform equivariance, the existing works of affine G-CNN are limited to transforms such as scaling, rotation, and reflection. So far, further including the shear transform is rarely considered in the conventional framework of affine G-CNN.

In addition, it has been shown that neural networks with greater depth and a larger number of parameters usually have better generalization performance [20], [21]. The heavy computational burden of one single group equivariant layer makes it difficult to apply parameter-sharing G-CNN to large neural network models. In this work, we show that the proposed efficient non-parameter-sharing G-CNNs can achieve superior performance to parameter-sharing G-CNNs when combined with advanced neural network architectures.

In this paper, we propose an efficient implementation of non-parameter-sharing G-CNNs based on an adaptive aggregation of Monte Carlo augmented decomposed filters. The contribution of this paper is embodied in four aspects:

- We propose an efficient non-parameter-sharing group equivariant network, where no additional channels or dimensions are introduced in implementing group convolution. Our method serves as an efficient extension of standard CNN. We give theoretical proof of how the group equivariance is achieved with conventional neural network training.
- Thanks to the convenience of weighted Monte Carlo (MC) sampling in implementation, our work can consider a more flexible mix of different simple transforms, we thereby introduce shear transform for affine G-CNN and demonstrate its potential to improve G-CNNs’ performance on natural images.
- Our non-parameter-sharing G-CNNs achieve superior performance to parameter-sharing-based G-CNNs when combined with advanced neural network architectures. Our approach does not increase the computation burden

and achieves high parameter and data efficiency compared with standard CNNs.

- With a set of suitable filter bases, the proposed networks serve as promising alternatives to standard CNNs for both image classification and image denoising tasks. Compared with standard CNNs, the proposed methods are good at exploiting large convolutional kernels efficiently, which helps build an efficient lightweight image-denoising network.

The paper is organized as follows: In the Methods section, we review the general framework of the group-equivariant model and introduce the details of our approach. We show the experimental results and discussions in the Experiments section and conclude the paper in the Conclusion section.

## II. METHODS

### A. The general framework of group-equivariant model

Group [22] is a classical mathematical concept, which is defined to be a set with a corresponding binary operation that is associative, contains an identity element, and has an inverse element for each element. In this paper, all the discussed groups are assumed to be locally compact groups. Following [3], we will briefly introduce the definition of group equivariant mapping and group convolution.

1) *Group equivariance*: In this paper, we consider a group  $G$  for the affine transformations on 2D images  $\mathbb{R}^2$ , which can be written as  $G = \mathbb{R}^2 \rtimes \mathcal{A}$ , a semidirect product between the translation group  $\mathbb{R}^2$  and another affine transform group  $\mathcal{A}$  (whose group element for 2D images takes the representation of a  $2 \times 2$  matrix). Its group product rule is defined as

$$\begin{aligned} g_1 \bullet g_2 &= (x_1, a_1) \bullet (x_2, a_2) \\ &= (x_1 + M(a_1)x_2, a_1 + a_2), \end{aligned} \quad (1)$$

where “ $\bullet$ ” denotes the group product operator,  $g_1 = (x_1, a_1)$ ,  $g_2 = (x_2, a_2)$  with  $x_1, x_2 \in \mathbb{R}^2$ ,  $a_1, a_2 \in \mathbb{R}^4$ , and function  $M: \mathbb{R}^4 \rightarrow \mathcal{A}$ . In this paper, we consider the following affine group, in particular, for any  $a = (\alpha, \sigma, s, r)$  with  $\alpha, \sigma, s \in \mathbb{R}$ ,  $M(a) = R(\theta)A(\alpha)S_1(s)S_2(r)$ , where

$$S_1(s) = \begin{bmatrix} 1 & s \\ 0 & 1 \end{bmatrix}, \quad (2)$$

$$S_2(r) = \begin{bmatrix} 1 & 0 \\ r & 1 \end{bmatrix}, \quad (3)$$

$$A(\alpha) = \begin{bmatrix} 2^\alpha & 0 \\ 0 & 2^\alpha \end{bmatrix}, \quad (4)$$

$$R(\theta) = \begin{bmatrix} \cos \theta & \sin \theta \\ -\sin \theta & \cos \theta \end{bmatrix}. \quad (5)$$

It should be noted that the existing works on affine G-CNN only consider translation, scaling, rotation, and mirror transforms. In this work, shear transform is included to form a more general case and explore its potential for boosting G-CNN’s performance on natural images.

For a group element of the affine transformation group  $g \in G$ , there is a corresponding group action on an index set  $\mathcal{X}$ ,

i.e., a transformation  $T : G \times \mathcal{X} \rightarrow \mathcal{X}$  for the index set. And for any  $g_1, g_2 \in G$  and  $x \in \mathcal{X}$ , we have

$$T(g_1 \bullet g_2, x) = T(g_1, T(g_2, x)). \quad (6)$$

The corresponding transformation  $\mathbb{T}_g$  for any function  $f : \mathcal{X} \rightarrow \mathbb{C}$  can be further defined as  $\mathbb{T}_g : f \rightarrow f'$  where  $f'(T(g, x)) = f(x)$ .

With the concept of group and group actions, we can now define the group equivariant map. Suppose we have a function  $f : \mathcal{X} \rightarrow V$  to be the input image or feature map of a neural network layer with  $V$  as a vector space. Let  $L_V(\mathcal{X})$  denote the Banach space of functions  $f : \mathcal{X} \rightarrow V$ . Consider a map  $\phi : L_{V_1}(\mathcal{X}_1) \rightarrow L_{V_2}(\mathcal{X}_2)$  between two function spaces  $L_{V_1}(\mathcal{X}_1) : \{f : \mathcal{X}_1 \rightarrow V_1\}$  and  $L_{V_2}(\mathcal{X}_2) : \{f : \mathcal{X}_2 \rightarrow V_2\}$ . For  $g \in G$ , we have  $T_g$  and  $T'_g$  to be  $G$  actions corresponding to set  $\mathcal{X}_1$  and  $\mathcal{X}_2$ , as well as  $\mathbb{T}_g$  and  $\mathbb{T}'_g$ . The map  $\phi$  is group equivariant if and only if

$$\forall g \in G, \phi(\mathbb{T}_g(f)) = \mathbb{T}'_g(\phi(f)) \quad (7)$$

2) *Group convolution*: A standard convolution of functions  $f$  with a kernel  $\psi : \mathbb{R} \rightarrow \mathbb{R}$ , is a translation-equivariant map, which can be written as

$$(\psi * f)(x) = \int \psi(-x + x')f(x')dx', \quad (8)$$

Group convolution is a generalization of standard convolution by introducing the group operation. The group convolution [3] [19] [23] [8] on a compact group  $G$  at group element  $g$  is written as

$$(\psi * f)(g) = \int_G \psi(g^{-1} \bullet g')f(g')d\mu(g') \quad (9)$$

where  $\mu$  is the Haar measure, and  $f, \psi : G \rightarrow \mathbb{C}$ . It should be noted that plain convolution is a special case of group convolution when only the translation group is considered (i.e.,  $g^{-1} = -x$ ;  $g' = x'$  and the "•" corresponds to "+"). [3] proved that the group convolution defined in equation (9) is a group-equivariant map.

### B. Adaptive aggregation of Monte Carlo augmented decomposed filters

In a discrete implementation of group convolution, the numerical integration is usually implemented based on the trapezoidal rule [24] using evenly sampled group elements  $g'$  in equation (9). For each input feature map channel (when considering many different kinds of affine transforms such as scaling, rotation, and mirror), nested integrals are needed, i.e. one nested integral per transform is considered. By this, the approach increases the computation burden exponentially with the number of considered transforms, which leads to the curse of dimensionality [25]. For example, when we have  $m$  different elements per transform and  $n$  transforms, this amounts to  $m^n$  terms to be evaluated.

To improve the flexibility of group convolution for the general affine transform group and avoid the curse of dimensionality, in this work, we propose to approximate the multi-dimensional integral over group operations in the group convolution by MC integration.

1) *Monte Carlo integration*: MC integration is known to tackle high-dimensional integration with robust convergence independent of the number of dimensions [25]. We consider for brevity only the standard MC variant, being aware that more efficient schemes such as Quasi-MC have the potential to substantially increase the performance further [26], [27].

For a multi-dimensional Monte Carlo integral, we have the theorem [28]–[30] as follows,

**Theorem II.1.** *Let  $\mu_p$  be a probabilistic measure on  $(\mathbb{R}^d, \mathcal{B}(\mathbb{R}^d))$ , i.e.,  $\mu_p(\mathbb{R}^d) = 1$ , and  $\mathcal{B}(\mathbb{R}^d)$  denotes the Borel algebra on  $\mathbb{R}^d$  with  $d$  the number of dimensions. For  $f \in L^2(\mathbb{R}^d, \mathcal{B}(\mathbb{R}^d), \mu_p)$ , we define*

$$I(f) = \int_{\mathbb{R}^d} f(x)d\mu_p(x), \quad (10)$$

and

$$Q_N(f) = \frac{1}{N} \sum_{i=1}^N f(\xi_i), \quad (11)$$

where  $(\xi_i)_{i \in \mathbb{N}}$  is an i.i.d sequence of random variables with distributions  $\mu_p$ . We have  $Q_N(f) \rightarrow I(f)$  when  $N \rightarrow +\infty$ . For all  $N \in \mathbb{N}$ , there is

$$(\mathbb{E}\|I(f) - Q_N(f)\|^2)^{1/2} = \sigma(f)/\sqrt{N}, \quad (12)$$

where  $\sigma^2(f) = I(f^2) - (I(f))^2$ , and  $\|\cdot\|$  is the  $l^2$  norm.

The Haar measure in (9) can be considered to be a corresponding probabilistic measure  $\mu_p$ . Therefore, it is theoretically justified to apply MC sampling for the discrete implementation of G-CNN.

2) *Discrete implementation of G-CNN with MC integration*: In the discrete implementation, we stochastically sample the group operations including, in our example, scaling, rotation, and shear transform. This approach allows a more flexible choice of the number of used transformations and decouples the relationship between the number of output channels and the number of categories of considered transformations.

Specifically, when we consider a filter  $W = w \cdot \psi$  with a fixed base filter  $\psi$  and  $w$  the trainable scalar weight, a continuous CNN layer can be written as

$$\begin{aligned} f_{c_o}^{(l+1)}(x) &= \sum_{c_i} w_{c_o, c_i}(\psi * f_{c_i}^{(l)})(x) \\ &= \sum_{c_i} \int_{\mathbb{R}^2} w_{c_o, c_i}^{(l)} \psi(u - x) f_{c_i}^{(l)}(u) du \end{aligned} \quad (13)$$

A corresponding discrete implementation of the convolutional layer<sup>1</sup> of  $l$ -th layer is as below

$$f_{c_o}^{(l+1)}(x) = \sum_{c_i} \sum_u w_{c_o, c_i}^{(l)} \psi(u - x) f_{c_i}^{(l)}(u) \quad (14)$$

where  $x, u \in \mathbb{R}^2$ ,  $\psi(\cdot)$  denotes the spatial convolutional filter function with a domain of translation group  $\mathbb{R}^2$ ,  $c_i \in [1, C_l]$  and  $c_o \in [1, C_{l+1}]$ .  $f_{c_i}^{(l)}(x)$  is the feature map of the  $l$ -th layer and  $w_{c_o, c_i}^l$  is the filter weight for the filter of the  $l$ -th layer with output channel  $c_o$  and input channel  $c_i$ .

<sup>1</sup>It should be noted that in this paper, for simplicity, we omit point-wise nonlinearity functions, constant scalar coefficients, and normalization layers in neural networks, which do not affect the group equivariance [3].

A continuous affine group equivariant CNN can be written as

$$\begin{aligned} f_{c_o}^{(l+1)}(g) &= \sum_{c_i} w_{c_o, c_i}^{(l)} (\psi * f_{c_i}^{(l)})(g) \\ &= \sum_{c_i} \int_G w_{c_o, c_i}^{(l)} \psi(g^{-1} \bullet g') f_{c_i}^{(l)}(g') d\mu(g') \end{aligned} \quad (15)$$

Let  $g = (x, a)$  and  $g' = (u, b)$ , we can rewrite the Haar integration in a group convolution of the  $l$ -th layer as:

$$\begin{aligned} f_{c_o}^{(l+1)}(x, a) &= \sum_{c_i} \int_{\mathbb{R}^4} \int_{\mathbb{R}^2} w_{c_o, c_i}^{(l)} 2^{-2\alpha_b} \cdot \\ &\psi(-x + M(-a)u, -a + b) f_{c_i}^{(l)}(u, b) dudb \end{aligned} \quad (16)$$

where we have the transform parameter vectors  $a = [\alpha_a, \theta_a, s_a, r_a]$ , and  $b = [\alpha_b, \theta_b, s_b, r_b]$ .

A typical corresponding discrete G-CNN can be written as below:

$$\begin{aligned} f_{c_o}^{(l+1)}(x, a) &= \sum_{c_i} \sum_b \sum_u w_{c_o, c_i}^{(l)} 2^{-2\alpha_b} \cdot \\ &\psi(-x + M(a)u, -a + b) f_{c_i}^{(l)}(u, b) \end{aligned} \quad (17)$$

In particular, the sum over the parameter vector  $b$  is a three-layer nested sum corresponding to the nested integrals in the continuous domain, which, as mentioned in previous sections, leads to a heavy computational burden.

The Monte-Carlo integration considers  $a$  and  $b$  as random variables. Suppose their entries  $\alpha = \xi_\alpha$ ,  $\theta = \xi_\theta$ ,  $s = \tan(\xi_s)$ , and  $r = \tan(\xi_r)$ , where  $\xi_\alpha$ ,  $\xi_\theta$ ,  $\xi_s$  and  $\xi_r$  are uniformly distributed in the range of  $[\eta_\alpha^1, \eta_\alpha^2]$ ,  $[-\eta_\theta, \eta_\theta]$ ,  $[-\eta_s, \eta_s]$ , and  $[-\eta_r, \eta_r]$ , respectively.

Suppose we draw  $N'$  samples of  $a$ , and  $N$  samples of  $b$ , respectively. The nested sum over  $b$  collapses into a one-dimension sum over  $N$  samples for MCG-CNN (Monte Carlo Group-equivariant CNN):

$$\begin{aligned} f_{c_o}^{(l+1)}(x, a_{n'}) &= \sum_{c_i} \sum_n \sum_u w_{c_o, c_i}^{(l)} 2^{-2\alpha_{b_n}} \cdot \\ &\psi(-x + M(-a_{n'})u, -a_{n'} + b_n) f_{c_i}^{(l)}(u, b_n) \end{aligned} \quad (18)$$

where  $n' \in \{1, \dots, N'\}$ , and  $n \in \{1, \dots, N\}$ .

3) *Adaptive aggregation of MC-augmented filters*: The Monte-Carlo approximation of G-CNN allows a flexible choice of the number of sampling points  $N$  per trainable weight  $w^{(l)}$  independent of the number of dimensions. However, compared with standard CNN, the computational burden of MCG-CNN is still  $N$  times larger. To eliminate the difference in computational burden between MCG-CNN and standard CNN, we propose WMCG-CNN (Weighted Monte Carlo Group-equivariant CNN)<sup>2</sup>, which reduces the number of transformations per input feature map channel (also per trainable weight)  $N$  to 1 and uses filter-weight-wise sampling instead. Specifically, we establish a one-to-one relationship between  $b$ ,  $c_o$  and  $c_i$ , as well as  $a$  and  $c_o$  by using  $c_o$  and  $c_i$  to index  $a$  and  $b$ . Thus we introduce notation  $b_{c_o, c_i}$  and  $a_{c_o}$ .

In this way, we yield WMCG-CNN with the equation (18) simplified into:

$$\begin{aligned} f_{c_o}^{(l+1)}(x, a_{c_o}) &= \sum_{c_i} \sum_u w_{c_o, c_i}^{(l)} 2^{-2\alpha_{b_{c_o, c_i}}} \cdot \\ &\psi(-x + M(-a_{c_o})u, -a_{c_o} + b_{c_o, c_i}) f_{c_i}^{(l)}(u, b_{c_o, c_i}), \end{aligned} \quad (19)$$

<sup>2</sup>The word "Weighted" in WMCG-CNN is used to emphasize that the number of trainable filter weights becomes transformation-wise in WMCG-CNN, which is thus an adaptive aggregation of augmented filters.

WMCG-CNN allows us to significantly increase the number of used transformations without increasing the computational burden, which, as shown in the later experiments, helps WMCG-CNN achieve superior performance to traditional discrete G-CNN.

However, due to the changes happening to WMCG-CNN, a question arises, i.e., under which circumstances, the WMCG-CNN can still be analogous to continuous G-CNN as the discrete G-CNN does? Below, we show that random initialization of the trainable weights can help the WMCG-CNN to be analogous to continuous G-CNN.

**Theorem II.2.** *Let  $f^{(l)}$  be an input feature map of the  $l$ -th layer with the number of channels  $C_l$ , and for each channel the number of spatial sampling points along vertical direction  $N_H$ , the number of spatial sampling points along horizontal direction  $N_W$ . A WMCG-CNN layer is group equivariant when the width of CNN,  $C_l \rightarrow \infty$ ,  $N_H \rightarrow \infty$ ,  $N_W \rightarrow \infty$ , and there exists a constant  $C < +\infty$  so that  $\|\int_{\mathbb{R}} wd\mu_w(w)\| < C$  with  $\mu_w$  a probabilistic measure on  $(\mathbb{R}, \mathcal{B}(\mathbb{R}))$  for the filter weight  $w$ , being a random variable.*

*Proof.* To prove the theorem, we have two steps: first, we construct a weighted integration function  $I$  and prove it is group equivariant. Then, we show that equation (19) corresponds to the discrete form of  $I$ .

1) Given  $g = (x, a_{c_o})$  and  $g' = (u, b)$ , we define the integration on  $\mathbb{R} \times G$  as

$$\begin{aligned} I(x, a_{c_o}) &= \int_{\mathbb{R} \times G} w \cdot \psi(g^{-1} \bullet g') f^{(l)}(g') d\mu(g') d\mu_w(w) \\ &= \int_{\mathbb{R}} \int_{\mathbb{R}^4} \int_{\mathbb{R}^2} w \psi(-x + M(-a_{c_o})u, -a_{c_o} + b) \\ &f^{(l)}(u, b) dudbdw \end{aligned} \quad (20)$$

Since  $\|\int_{\mathbb{R}} wd\mu_w(w)\| < C$ , we have the constant  $C_w = \int_{\mathbb{R}} wd(w)$ . Thus

$$\begin{aligned} I(x, a_{c_o}) &= C_w \cdot \int_{\mathbb{R}^4} \int_{\mathbb{R}^2} \psi(-x + M(-a_{c_o})u, -a_{c_o} + b) \\ &f^{(l)}(u, b) dudb \end{aligned} \quad (21)$$

which is group equivariant.

2) Let  $q(x, a_{c_o}, b) = \int_{\mathbb{R}^2} \psi(-x + M(-a_{c_o})u, -a_{c_o} + b) f^{(l)}(u, b) du$ , so we have

$$I(x, a_{c_o}) = \int_{\mathbb{R}} \int_{\mathbb{R}^4} w q(x, a_{c_o}, b) dbdw \quad (22)$$

Now, we consider the transition from continuous to discrete formulations. Since both  $w$  and  $b$  are independently randomly sampled with the samples indexed by  $c_i$ . According to Theorem II.1, we have

$$I(x, a_{c_o}) = \lim_{C_l \rightarrow \infty} \frac{1}{C_l} \sum_{c_i} w_{c_o, c_i}^{(l)} q(x, a_{c_o}, b_{c_o, c_i}) \quad (23)$$

Since  $u$  is sampled based on the trapezoidal rule, we have

$$\begin{aligned} q(x, a_{c_o}, b_{c_o, c_i}) &= \lim_{N_H \rightarrow +\infty} \lim_{N_W \rightarrow +\infty} \frac{1}{N_H N_W} \sum_u 2^{-2\alpha_{b_{c_o, c_i}}} \cdot \\ &\psi(-x + M(-a_{c_o})u, -a_{c_o} + b_{c_o, c_i}) f_{c_i}^{(l)}(u, b_{c_o, c_i}), \end{aligned} \quad (24)$$

Meanwhile, we rewrite the corresponding convolution part of WMCG-CNN equation (19) as

$$\begin{aligned} f_{c_o}^{(l+1)}(x, a_{c_o}) &= \frac{1}{C_l N_H N_W} \sum_{c_i} \sum_u w_{c_o, c_i}^{(l)} 2^{-2\alpha_{b_{c_o, c_i}}} \cdot \\ &\psi(-x + M(-a_{c_o})u, -a_{c_o} + b_{c_o, c_i}) f_{c_i}^{(l)}(u, b_{c_o, c_i}), \end{aligned} \quad (25)$$

where  $c_i \in \{1, 2, \dots, C_l\}$ ,  $u = (u_1, u_2)$  with  $u_1 \in \{1, 2, \dots, N_H\}$  and  $u_2 \in \{1, 2, \dots, N_W\}$ . Here we include coefficient  $\frac{1}{C_l N_H N_W}$  so that  $f_{c_o}^{(l+1)}$  is the average of the samples.

Therefore, by combining (23) and (24), we have

$$\begin{aligned} I(x, a_{c_o}) &= \lim_{C_l \rightarrow \infty} \lim_{N_H \rightarrow +\infty} \lim_{N_W \rightarrow +\infty} f_{c_o}^{(l+1)}(x, a_{c_o}) \end{aligned} \quad (26)$$

The proof is completed.  $\square$

As we know, random initialization of trainable weights is a common strategy adopted in most existing state-of-the-art deep learning methods. Theorem II.2 proves that the random weight initialization strategy together with the MC-augmented filters can help raise the CNN to a good starting point before training with an optimization algorithm, which therefore makes it easier for the network to find the optimal solution. This starting point is a network that approximately satisfies convolutional-layer-wise group equivariance. Obviously, a necessary condition of an optimal solution is that in contrast to the approximate convolutional-layer-wise group equivariance, it is at least at the level of the entire neural network that the group equivariance is achieved approximately.

From Theorem II.1, we know that the convergence speed of the Monte Carlo integration is slow. When the number of samples is small, the variance may not be satisfactory. However, with the weight  $w$  as learnable parameters and the samples of transformations fixed, the neural network can learn optimal weight distribution to improve the group equivariance, which will be shown in the later experiments (Fig. 4). Accordingly, we can rewrite equation (23) as follows:

$$\begin{aligned} I(x, a_{c_o}) &= \lim_{C_l \rightarrow \infty} \frac{1}{C_l} \sum_{c_i} w_{c_o, c_i}^{(l)} q(x, a_{c_o}, b_{c_o, c_i}) \\ &\approx \hat{I}(x, a_{c_o}) = \frac{1}{C_l} \sum_{c_i} w_{c_o, c_i}^{(l)} q(x, a_{c_o}, b_{c_o, c_i}) \end{aligned} \quad (27)$$

The estimator  $\hat{I}$  in equation (27)) has a similar form to that of the conventional importance sampling method [31]. The differences are that the weight distribution in WMCG-CNN is not manually designed but is learned by iterative data-driven optimization algorithms for neural networks instead, and the learned weights may not be considered being i.i.d. random.

Assuming  $I$  a unique constant for the given  $x$  and  $a_{c_o}$ , we have the variance  $Var(\hat{I} - I) = Var(\hat{I})$ . We know that the variance of the estimator  $\hat{I}$  is reduced during the training when the training process leads to affine equivariance with  $Var(\hat{I} - I) \rightarrow 0$ . Such a training process usually requires rich affine transformations existing in the image sets. This requirement is usually met in practice because the affine transformations are common in natural images. Moreover, affine-transformation-based data augmentation is also a common training technique to achieve this.

In addition to factors during training, in practice, certain fundamental structural features of neural networks also help ensure training stability and low variance. Specifically, when applying WMCG-CNN, multiple bases are often used. This increases the diversity of the filters. Furthermore, residual connections are used in each bottleneck block of the hidden

layer to avoid information loss and instability, which is common in most modern neural network architectures. Residual connections also implicitly increase the number of samples, as they transmit the same input to the next layer to be processed by more filters. Therefore, when using our method on the hidden layers of neural networks with residual connections, we generally do not need to worry about its stability.

4) *Filter decomposition and the relationship to traditional CNN filters:* In the previous section, we only consider one basis filter function  $\psi$ , to increase the expressiveness of networks, we adopt the filter decomposition approach to build convolutional filters by the sum of multiple weighted filter bases. Specifically, we have  $W_{c_o, c_i}^{(l)}(x, a) = \sum_j w_{c_o, c_i, j}^{(l)} \tilde{\psi}_j(x, a)$  with  $\tilde{\psi}_j(x, a)$  an orthogonal basis function with  $x \in \mathbb{R}^2$  and  $a \in \mathbb{R}^4$  the transform parameter vector,  $w_{c_o, c_i, j}^{(l)}$  the trainable weights,  $j \in [1, K]$ , and  $K$  the chosen number of basis functions. In the proposed WMCG-CNN, according to equation (19) the WMCG-CNN can be written in a similar way to the standard CNN in equation (14) as below:

$$\begin{aligned} f^{(l+1)}(c_o, x, a_{c_o}) &= \sum_{c_i} \sum_u 2^{-2\alpha_{b_{c_o, c_i}}} W_{c_o, c_i}^{(l)}( \\ &-x + M(-a_{c_o})u, -a_{c_o} + b_{c_o, c_i}) f_{c_i}^{(l)}(u, b_{c_o, c_i}), \end{aligned} \quad (28)$$

In the practical discrete implementation, the choice of filter basis can be various. For different datasets and different tasks, the optimal filter basis can be different. In the following experiments, we generally adopt two kinds of filter basis: the Fourier-Bessel (FB) basis [32], and the continuous Mexican hat (MH) wavelet basis [33], [34]. The scaling, rotation, and shear transformations are used to augment the FB filters. The MH filters are augmented by scaling, translation, and shear transformations. Supposing any filter basis is a matrix of size  $k \times k$ , for FB basis, we can have  $k^2 - 1$  non-constant bases and a constant scalar basis at the most.

The 2D MH filters can be written as

$$\psi(\sigma_x, \sigma_y, x, y) = \frac{1}{2\pi\sigma_x\sigma_y} \left[ 2 - \frac{x^2}{\sigma_x^2} - \frac{y^2}{\sigma_y^2} \right] e^{-\frac{x^2}{2\sigma_x^2} - \frac{y^2}{2\sigma_y^2}} \quad (29)$$

The peak frequency of the MH wavelet function  $f_x = \frac{1}{\sqrt{2\pi}\sigma_x}$  and  $f_y = \frac{1}{\sqrt{2\pi}\sigma_y}$  [35], which can be used for scaling along  $x$  or  $y$  axis.

It should be noted that when using the bases consisting of translation-augmented discrete Dirac delta functions, the proposed methods fall back into standard CNN filters. Figure 2 shows examples of different filter bases.

In addition, theoretically, in the training phase, the computational burden of the proposed method is slightly higher than that of the corresponding standard CNN that uses the same size of the convolutional kernel (as shown in Table I). This is because of the weighted sum of filter bases. Yet, the weighted sum can be pre-calculated with the results stored in memory before doing an inference. Thus, in the inference phase, the network using the proposed method has exactly the same computational complexity as the corresponding standard CNN.

### C. Extending to discrete groups with bootstrap resampling

In the previous sections, we focus on continuous groups and how the weighted G-CNN can be approximated with the

TABLE I

THE COMPUTATIONAL TIME AND MEMORY USAGE ON GPU NVIDIA A100 40GB FOR CNN MODELS TRAINED ON IMAGENET DATASET, WHERE BOTH CNN AND OUR WMCG-CNN MODELS ARE USING THE SAME KERNEL SIZE AND THE SAME NUMBER OF LEARNABLE PARAMETERS.

Base model	ResNeXt50		ResNet50		ConvNeXt-S	
	CNN	WMCG-CNN	CNN	WMCG-CNN	CNN	WMCG-CNN
Training Time (s/epoch)	3884	3914	2793	2808	4739	4754
Training VRAM Footprint (MB)	35078	35116	24934	25106	25742	25990

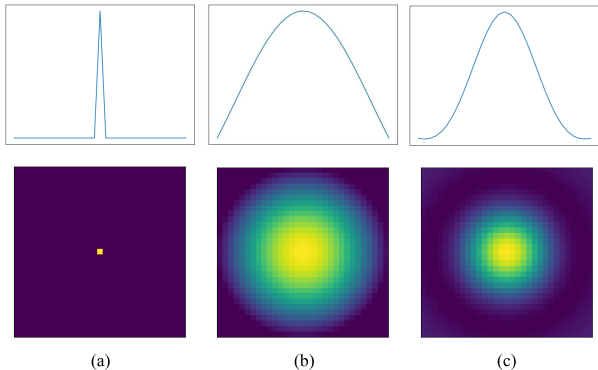


Fig. 2. Examples of filter bases in 1-dimension and 2-dimension space. (a) the discrete Dirac delta basis, (b) the Fourier Bessel basis; (c) the Mexican hat basis.

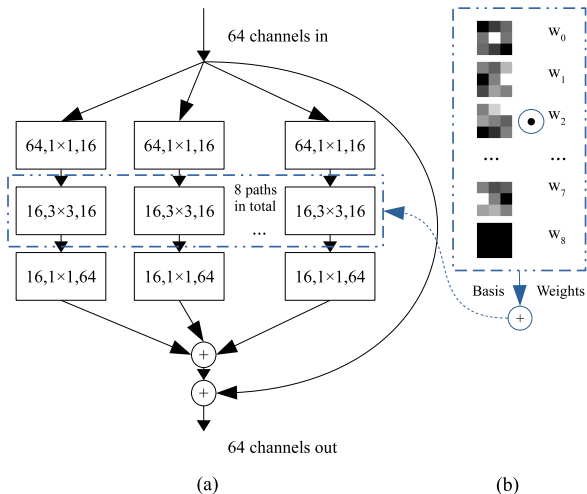


Fig. 3. Integrating the proposed WMCG-CNN into the classic bottleneck architecture. (a) The example bottleneck block with group convolution using  $3 \times 3$  filters; (b) An example of filter composition with MC-augmented basis.

discretized implementation assuming an infinite number of filter samples. However, our method can also apply to cases where the number of available group elements is far less than the number of input-output channel pairs (in equation (19)). We can use the bootstrap resampling [36] method to make the number of augmented basis samples large enough to match each weighted input-output channel pair.

#### D. Integrating WMCG-CNN into the existing state-of-the-art CNN architectures

We see that when  $\tilde{\psi}_j$  degenerates to a scalar, i.e. a  $1 \times 1$  base filter, the convolution is obviously exactly group equivariant,

while on the other hand, the non-scalar filter  $\tilde{\psi}_j$  requires a huge number of sampling points to approximate the continuous G-CNN. To leverage the advantage of  $1 \times 1$  base filters, one can add  $1 \times 1$ -filter-based convolution layers as a secondary adaptive aggregation of features from the output channels of WMCG-CNN. By combining the  $1 \times 1$  layer with the  $k \times k$  convolution layer into a single unit or block, the total number of considered transformations is increased from  $C_l$  to  $C_{l+1}C_l$  (i.e., the number of all the  $k \times k$  filters used in the  $l$ -th layer) with a relatively small increase of the number of parameters. In addition, the  $1 \times 1$  CNN layer also helps to enrich the design space for WMCG-CNN, where the use of the small  $1 \times 1$  kernel helps to achieve a high parameter efficiency given the same level of expressiveness and the same number of parameters [37].

Interestingly, the secondary aggregation with a cascaded  $1 \times 1$  convolutional layer is intrinsically similar to the bottleneck architecture that is adopted in all the state-of-the-art CNNs derived from ResNet [37]. The only difference is that the bottleneck architecture uses one extra  $1 \times 1$  convolution layer before the  $k \times k$  convolution layer.

Apart from  $1 \times 1$  layers, we also note that the channel grouping convolution technique<sup>3</sup> proposed in ResNeXt [38] is also a helpful technique for improving CNN’s performance.

Thanks to the flexibility of the proposed WMCG-CNN, we can easily combine these techniques with the WMCG-CNN. An example is shown in Fig. 3. Similar blocks but with different filter sizes will be used in later image denoising experiments.

### III. EXPERIMENTS

We test WMCG-CNN on classification and regression tasks, such as image classification and image denoising. In the image classification part, we also conducted ablation experiments, and compared our method with the parameter-sharing group equivariant methods.

#### A. Performance metrics

We adopt the following performance metrics: the number of trainable parameters in million ( $10^6$ ), Params(M); the number of Multiply–Accumulate Operations in giga ( $10^9$ ), MACs(G); the prediction error in percentage, Error(%); mean prediction error on corrupted validation image datasets in percentage, mCE(%); top 1 accuracy in percentage, top-1 acc.(%); top 5 accuracy in percentage, top-5 acc.(%); peak signal-to-noise

<sup>3</sup>It should be noted that here the channel group is a concept that differs from the transformation group. The channel grouping convolution technique divides the input feature map channels into multiple channel groups of the same width to perform convolution operations separately.

ratio in dB, PSNR(dB); the degree of parameter-sharing, MACs/Params (G/M).

In addition, for the section of the ablation experiments, similar to [39], we define mean normalized group-equivariant error (mGE) according to equation (7):

$$mGE = \mathbb{E}(\|\phi(\mathbb{T}_g(f)) - \mathbb{T}'_g(\phi(f))\|/\|\phi(\mathbb{T}_g(f))\|) \quad (30)$$

where for each input image, a random affine transformation  $g \in G$  is selected with the shear range  $[-0.5\pi, 0.5\pi)$ , the scaling range  $[1.0, 2.0)$  and rotation angle range  $[-1.0\pi, 1.0\pi)$ .

### B. Ablation experiments

For ablation experiments, we consider a subset of the ImageNet1k dataset. ImageNet1k has 1.28 million color images for 1,000 different classes from WordNet. The validation dataset consists of 50,000 images. For quick experiments, we extract the first 40 classes for ablation experiments (i.e., from class *n01440764* to class *n01677366*), and thus we denote the corresponding datasets as ImageNet40. We scale all the images to  $224 \times 224$  resolution and normalize images in a classic way. The prediction Error (%) is used to measure the classification performance.

We use ResNet18, ResNet50, and ResNeXt50 [38] as the baseline networks. We follow the state-of-the-art robust training methods as in [40]. The neural networks are trained for 90 epochs with an initial learning rate of 0.01 following a cosine decay schedule. The Pixmix augmentation technique is used with its default setting as in [40]. Pixmix uses affine transformations (including translation, rotation, and shear transform) as well as other augmentation methods to generate augmented clean images. As for WMCG-CNN, we replace all the hidden non- $1 \times 1$  CNN layers with the proposed WMCG-CNN layers. By default, the size of FB basis is  $5 \times 5$ , the number of basis per filter is 9 (We have the number of bases per filter 9 (the first 9 low frequency Bessel filters), the scaling range is  $[1.0, 2.0)$ , the rotation angle range  $[-2\pi, 2\pi)$ , and the shear transform angle range  $[-0.25\pi, 0.25\pi)$ . In this work, considering the symmetry of the filter basis, by default, we keep the shear angle of  $S_2(r)$  as zero for simplicity. For convenience, we name each version of the tested networks with a series of suffixes. Specifically, "kn" means the filter size is  $n \times n$ . In the experiments with shear transforms, we use the suffix "shear- $n_s\pi$ " to denote shear transform angle  $[-n_s\pi, n_s\pi)$ . We change the value of  $n_s$  from 0.00 to  $0.50\pi$  to test the effect of the shear transform. In particular,  $n_s = 0.00$  means that there is no shear transform applied. The suffix "WT" means that the MH wavelet filter basis is used. The suffix "not" means that there is no translation augmentation used in the experiments with the MH wavelet. In addition, with ResNet18 as a baseline network, we also tested the conventional parameter-sharing scale-equivariant CNN, and the proposed MC scale-equivariant CNN. The suffix "scale- $n$ " means the use of  $n$  scaling transformation  $\alpha = \{0, 1/n, 2/n, \dots, (n-1)/n, 1\}$ . The suffix "MC-scale- $n$ " means using  $n$  MC-augmented scaling transformations. The suffix "MC-affine- $n$ " means using  $n$  affine (scaling-rotation-shear) transformations. For the implementation of "scale- $n$ ", "MC-scale- $n$ ", and "MC-affine- $n$ ", we draw  $n$  samples of

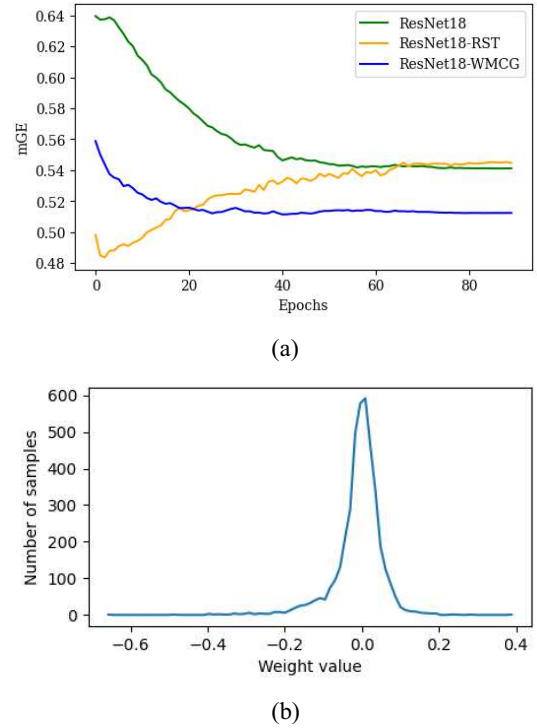


Fig. 4. (a) The mGEs of the first hidden CNN layer with 256 input and output channels of different residual networks for 90 epochs of training on ImageNet dataset. (b) The histogram of the learned weights for the FB basis of order 0 in the first hidden CNN layer of ResNet18-k5-WMCG-shear-0.25 $\pi$ .

transformation for the input feature map, and we only have 1 sample of transformation for the corresponding output feature map to avoid the computational burden from becoming too heavy. "width1/n" means that the total width of output feature maps is reduced to  $1/n$  by decreasing the number of channels per transformation. "nb  $n$ " means  $n$  basis used per filter. "nb1- $n$ " means using only one Bessel basis with the  $(n+1)$ -th lowest frequency (excluding the constant scalar basis).

Fig. 4a shows the mGE results for the first hidden CNN layer with 256 input and output channels of ResNet18, ResNet18-RST, and ResNet18-WMCG-shear-0.25 $\pi$  for the 90-epoch training on ImageNet dataset. For all the ResNet18 variants, the hidden  $3 \times 3$  CNNs layers are replaced with a corresponding  $5 \times 5$  CNNs. The  $5 \times 5$  CNN layers of ResNet18-RST are RST-CNNs [16]. We see that compared with the plain CNNs and RST-CNNs, WMCG-CNNs achieve the lowest mGE after 90 epochs of training. The mGE of RST-CNN initially drops sharply but increases gradually to a high value. This implies that the parameter-sharing strategy helps reduce mGE more quickly in the initial stages but may not boost the equivariance in the following training iterations. Figure 4b shows that the distribution of the learned weights is centered around zero.

Fig. 5 shows the output feature maps of the plain CNN, RST-CNN [16], and our WMCG-CNN for affinely transformed input images. All the CNNs consist of the classic two layers structure in bottleneck block of ResNet, where the first convolution layer has a kernel size of  $5 \times 5$ , 3 input channels, and 256 output channels, and the second layer is of kernel size  $1 \times 1$

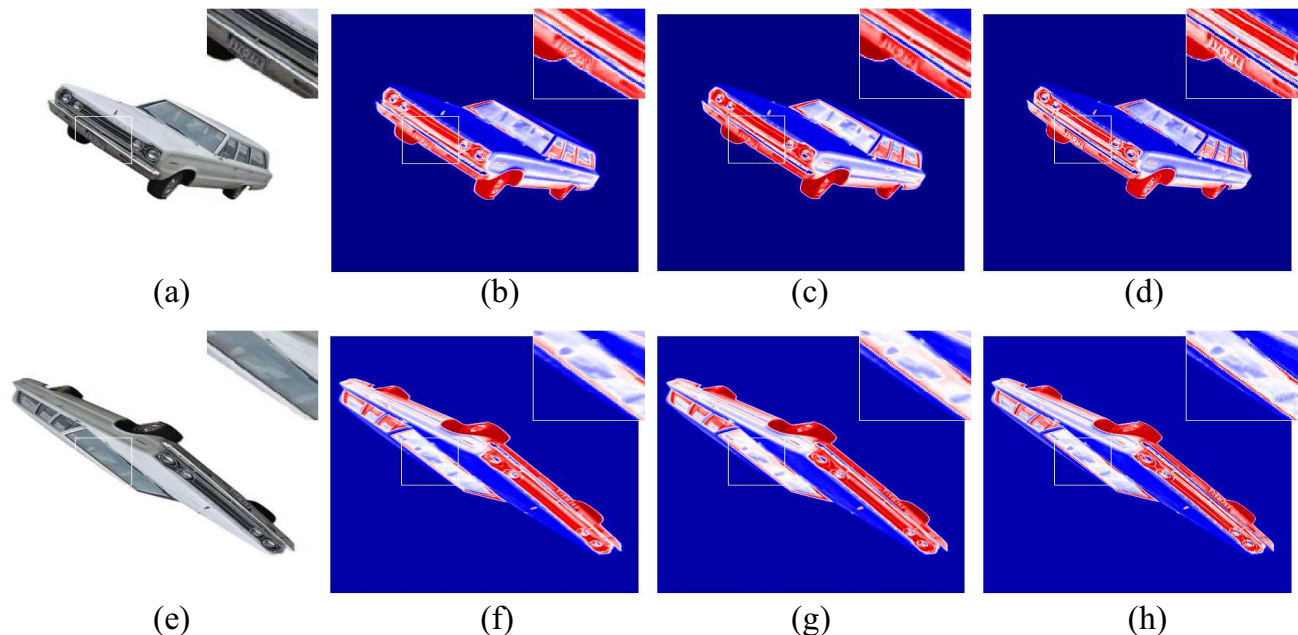


Fig. 5. The output feature map of CNNs for affinely transformed inputs. The original input image is cropped from a car image selected from STL10 [41] dataset. The areas in the white rectangular boxes are upscaled to show the details. (a) Input 1; (b) The output of plain CNN for Input 1; (c) The output of RST-CNN for Input 1; (d) The output of WMCG-CNN for Input 1; (e) Input 2; (f) The output of plain CNN for Input 2; (g) The output of RST-CNN for Input 2; (h) The output of WMCG-CNN for Input 2.

with 1 output channel. The  $1 \times 1$  convolutional layers for both CNNs have the same weights. We see that the output features of our WMCG-CNN have clearer edges and richer details. Compared with the plain CNN with Dirac delta bases and the RST-CNN with Fourier Bessel bases, our WMCG-CNN with Fourier Bessel bases performs better in retaining image details and is therefore helpful for boosting affine equivariance.

Table II shows the results of ablation experiments on ImageNet40, where the results with respect to Params(M) and MACs(G) are also displayed. We see that the shear transform with a suitable range shear angle is helpful for increasing WMCG-CNN’s performance. In all the following experiments, we adopt  $n_s = 0.25$  for FB basis and  $n_s = 0.5$  for the MH basis by default if not explicitly stated. It should be noted that the MH basis additionally uses translation augmentation that proves to help increase its performance.

About the results with different versions of ResNet18-WMCG-k5-nb1, we see the choice of FB basis affects the prediction performance significantly. Low-frequency basis, i.e., Bessel basis of low order, is shown to be more important than high-frequency basis. Therefore, to select a fixed number of bases, we must include the low-order Bessel basis first.

The conventional scale-equivariant CNN architecture ResNet18-k5-scale-4 has a decent prediction error. However, the computational burden is extremely high. When we try to reduce the computational burden by decreasing the width of the network to get ResNet18-k5-scale-4-width1/4, the number of trainable parameters is reduced significantly which leads to poorer prediction performance. The MCG-CNN also has a heavy computational burden and is superior to its corresponding G-CNN when we use a larger number of transformations and more transformation types (such as ResNet18-k5-MC-

affine-16-width1/16).

Among the tested ResNet baseline architectures, the results with ResNet18 give the lowest mean error, which indicates that the deeper models such as ResNet50 and ResNeXt50 suffer from over-fitting because the number of classes is reduced from 1k to 40. However, the WMCG-CNN can reduce the over-fitting consistently for all the considered baseline models. WMCG-CNN versions of ResNet18 yield the best classification performance. Generally, the results on ImageNet40 demonstrate that, with suitable filter bases, WMCG-CNN is superior to standard CNN in sample efficiency, helps avoid over-fitting, and enables a quicker convergence.

### C. Comparison with the state-of-the-art parameter-sharing G-CNNs

We test all the group equivariant networks on three common small-scale datasets, Rotated-Scaled-and-Sheared MNIST (RSS-MNIST), CIFAR10 [42], and STL10 [41]. The original MNIST dataset [43] consists of 70,000  $28 \times 28$  images of handwritten digits. Similar to [16], RSS-MNIST is constructed through randomly rotating (by an angle uniformly distributed on  $[0, 2\pi]$ ), shearing (by an angle uniformly distributed on  $[-\pi/4, \pi/4]$ ) as well as rescaling (by a uniformly random factor from  $[0.3, 1]$ ) the original MNIST [43] images. The transformed images are zero-padded back to a size of  $28 \times 28$ . We upsize the image to  $56 \times 56$  for better comparison of the models. The CIFAR-10 dataset consists of color images of size  $32 \times 32 \times 3$  for 10 classes. There are 50,000 training images and 10,000 testing images. The STL10 dataset consists of 13,000 RGB images of size  $96 \times 96$  belonging to 10 different classes, including 5,000 images for training set and 8,000 for test set. Similar to [16], we evaluate different models

TABLE II  
THE ABLATION EXPERIMENTS ON THE IMAGENET40 DATASET FOR DIFFERENT RESIDUAL NETWORKS.

Model	Params (M)	MACs (G)	Error (%)
ResNet18 [37]	11.69	1.82	24.85
ResNet18-k3-WMCG-shear-0.25 $\pi$ <sup>a,b</sup>	11.69	1.82	<b>22.45</b>
ResNet18-WT-k3-WMCG-shear-0.00 <sup>c</sup>	11.69	1.82	25.10
ResNet18-WT-k3-WMCG-shear-0.12 $\pi$	11.69	1.82	<b>24.55</b>
ResNet18-WT-k3-WMCG-shear-0.25 $\pi$	11.69	1.82	26.85
ResNet18-WT-k3-WMCG-shear-0.50 $\pi$	11.69	1.82	25.10
ResNet18-WT-k3-WMCG-shear-0.50 $\pi$ -not <sup>d</sup>	11.69	1.82	25.85
ResNet18-k5-WMCG-shear-0.00	11.69	4.80	19.60
ResNet18-k5-WMCG-shear-0.12 $\pi$	11.69	4.80	<b>18.80</b>
ResNet18-k5-WMCG-shear-0.25 $\pi$	11.69	4.80	19.20
ResNet18-k5-WMCG-shear-0.40 $\pi$	11.69	4.80	19.40
ResNet18-k5-scale-4 <sup>e</sup>	11.69	18.77	19.80
ResNet18-k5-scale-16-width1/4 <sup>f</sup>	11.69	18.77	19.00
ResNet18-k5-MC-scale-16-width1/4 <sup>g</sup>	11.69	18.77	19.20
ResNet18-k5-MC-affine-16-width1/4 <sup>h</sup>	11.69	18.77	<b>18.90</b>
ResNet18-k5-scale-4-width1/4	3.45	4.80	<b>24.45</b>
ResNet18-k5-MC-scale-4-width1/4	3.45	4.80	24.90
ResNet18-k5-MC-affine-4-width1/4	3.45	4.80	24.55
ResNet18-k5-scale-16-width1/16	1.39	4.80	35.50
ResNet18-k5-MC-scale-16-width1/16	1.39	4.80	36.75
ResNet18-k5-MC-affine-16-width1/16	1.39	4.80	<b>32.65</b>
ResNet18-k5-WMCG-nb1-r0 <sup>i</sup>	1.92	4.80	<b>28.65</b>
ResNet18-k5-WMCG-nb1-r2	1.92	4.80	32.05
ResNet18-k5-WMCG-nb1-r7	1.92	4.80	55.45
ResNet50 [37]	25.56	4.12	29.35
ResNet50-k5-WMCG-shear-0.25 $\pi$	25.56	7.41	<b>22.20</b>
ResNeXt50 [38]	25.03	4.27	27.00
ResNeXt50-k5-WMCG-shear-0.00	25.03	4.68	27.60
ResNeXt50-k5-WMCG-shear-0.12 $\pi$	25.03	4.68	27.00
ResNeXt50-k5-WMCG-shear-0.25 $\pi$	25.03	4.68	<b>26.95</b>
ResNeXt50-k5-WMCG-shear-0.40 $\pi$	25.03	4.68	27.90

Note: a) "kn" means the filter size of hidden non-1  $\times$  1 convolutional layers is  $n \times n$ .  
 b) "shear- $n_s\pi$ " denotes shear transform angle  $[-n_s\pi, n_s\pi]$ .  $n_s = 0.00$  means that there is no shear transform applied.  
 c) The suffix "WT" means that the MH wavelet filter basis is used.  
 d) The suffix "not" means no translation augmentation is used in the experiments with the MH wavelet.  
 e) The suffix "scale- $n$ " means the use of  $n$  scaling transformation  $\alpha = \{0, 1/n, 2/n, \dots, (n-1)/n, 1\}$ .  
 f) "width1/ $n$ " means that the total width of output feature maps is reduced to  $1/n$  by decreasing the number of channels per transformation.  
 g) The suffix "MC-scale- $n$ " means using  $n$  MC-augmented scaling transformations.  
 h) The suffix "MC-affine- $n$ " means using  $n$  affine (scaling-rotation-shear) transformations.  
 i) "nb  $n$ " means  $n$  bases used per filter. "nb1- $r$ " means using only one Bessel basis with the  $(n+1)$ -th lowest frequency (excluding the constant scalar basis).

under both in-distribution (ID) and out-of-distribution (OOD) settings. Specifically, the training set remain unchanged. The ID setting keeps the test set unchanged. The OOD setting augment the test set with uniform random affine transformations with scaling range  $[0.9, 1.1)$ , rotation angle range  $[0, 0.1\pi)$ , and shear transform angle range  $[0, 0.1\pi)$  along vertical and horizontal directions.

About experiments on RSS-MNIST dataset, following the test procedure for group equivariant networks described in [16], [44], [45], we generate six independent realizations of augmented data. Each of them is split into three parts: 10,000 images for training, 2,000 for validation, and 50,000 for testing. Adam optimizer is used to train all models for 60 epochs with the batch size set as 128. The initial learning rate is 0.01 and decreases tenfold after 30 epochs. We compare methods with the state-of-the-art parameter-sharing group equivariant network, attentive G-CNN [17] and RST-CNN [16]. The implementation of the proposed method uses the same filter basis as RST-CNN. Since the number of their basis is much limited, we use the bootstrap resampling method to obtain an enough number of bases. We use modified versions of ResNeXt50 as baseline networks. Specifically, we first removed the first pooling layer, and all the convolutional layers

with a stride size of two are replaced with a corresponding convolutional layer with a stride size of one concatenated with a max-pooling layer. Then we have ResNeXt50-k7 by replacing all the non-1  $\times$  1 kernels with 7  $\times$  7 kernel. We build ResNext-k15-base by further replacing the 7  $\times$  7 kernels in the first three stages of ResNeXt50-k7 with 15  $\times$  15 kernels. Finally, we get ResNeXt50-WMCG-k15 by replacing all 15  $\times$  15 hidden convolutional layers of ResNext-k15-base with the proposed WMCG convolutional layers using bootstrap resampled 15  $\times$  15 basis.

We also show comparison results with attentive G-CNN [17] and efficient group equivariant network [8] on CIFAR10 datasets. The networks from [17] are trained in the same way as our methods. Since [8] does not publish their code, we simply refer to the results in their paper directly.

For experiments on CIFAR10 dataset [42], we use ResNeXt29 (32  $\times$  4) [38] as the baseline network. We denote "ResNeXt29-FB-k3-WMCG-nb9" as the network created by replacing the 3  $\times$  3 convolution layer with WMCG CNN of the 3  $\times$  3 FB basis size and each convolutional filter using 9 bases. Empirically, only for the experiments with CIFAR10 dataset, we use scaling range  $[1.0, 1.5)$ , while in other experiments we keep  $[1.0, 2.0)$ . Apart from FB basis, we also tested the augmented continuous MH wavelet filter as the basis for WMCG CNN. We denote "ResNeXt29-WT-k3-WMCG-nb9" as the network created by replacing the 3  $\times$  3 convolution layer with WMCG CNN of the 3  $\times$  3 MH basis size and each convolutional filter using 9 bases. The filter basis is augmented with translation, scaling, and shear transforms.

All the CNNs are trained with the same training strategy as in [46]. Specifically, all the networks are trained using an initial learning rate of 0.1 and a cosine learning rate schedule. The optimizer uses stochastic gradient descent with Nesterov momentum and a weight decay of 0.0005. The input images are first pre-augmented with standard random left-right flipping and cropping, and then the Augmix method [46] is applied with its default settings. Augmix uses affine transformations (including translation, rotation, and shear transform) as well as other augmentation methods to generate augmented clean images. We repeat the training-and-testing experiments for six rounds and report the mean results  $\pm$  standard deviation.

For experiments on STL10 dataset [41], all the CNNs are trained using an initial learning rate of 0.05 and batch size 64 for 1,000 epochs. Following [16], the learning rate The optimizer uses stochastic gradient descent with Nesterov momentum and a weight decay of 0.0005. The learning rate decays by 0.2 at epoch 300, 400, 600 and 800, respectively. The experiments repeat for 6 times and report the mean results  $\pm$  standard deviation. We compare methods with the state-of-the-art parameter-sharing group equivariant network, SESN [12] and RST-CNN [16] on STL10. The implementation of the proposed method uses the same filter basis as SESN [12]. Since the number of their basis is much limited, we use the bootstrap resampling method to obtain an enough number of bases. We use modified versions of ResNeXt50 as baseline networks. Specifically, the width of the bottleneck blocks is doubled. The hidden non-1  $\times$  1 convolution layers have a kernel

of size  $7 \times 7$ . The last 3 Bottleneck blocks are removed and the last fully connected layer is therefore adapted with input channel number the same as that of the output of nearest remaining bottleneck block. The output channel number of first convolutional layer is increased to 4 times followed by a  $1 \times 1$  convolution layer for adaptation of the output channel number. The first pooling layer is removed. We denote the modified ResNet50 as "ResNet50-k7".

Table III shows the results of compared G-CNNs on RSS-MNIST and CIFAR10. We see that the WMCG networks outperform the parameter-sharing networks with much less computational burden while not increasing the computational burden of standard CNNs. The MACs/Params results show that the proposed method has almost the same level of parameter-sharing as the standard CNNs. We also note that FB basis used to perform well on ImageNet datasets but obtained poor performance on CIFAR10 datasets. On the other hand, the wavelet basis which used to work poorly on ImageNet surpasses FB basis on CIFAR10.

TABLE III

THE COMPARISON RESULTS OF IMAGE CLASSIFICATION EXPERIMENTS WITH PARAMETER-SHARING GROUP EQUIVARIANT NEURAL NETWORK MODELS ON MNIST AND CIFAR10 DATASETS.

Model	RSS-MNIST			
	Params (M)	MACs (G)	MACs/Params (G/M)	Error (%)
mnist_CNN_56 [16]	0.49	0.14	0.29	8.76±0.11
romhog_fa_p4cnn [17]	0.02	0.02	0.63	8.07±0.17
RST-CNN <sup>a</sup> [16]	3.24	5.68	1.75	4.96±0.10
ResNeXt50 [38]	25.03	4.27	0.17	7.70±0.48
ResNeXt50-k7 <sup>b</sup>	14.42	2.26	0.16	5.27± 0.42
ResNeXt50-k15-base	14.82	2.60	0.18	6.31± 0.33
ResNeXt50-WMCG-k15	14.42	2.60	0.18	<b>4.81± 0.19</b>
Model	CIFAR10			
	Params (M)	MACs (G)	MACs/Params (G/M)	Error (%)
ALL-CNN- $\alpha_F$ -p4m [17]	1.25	2.92	2.34	6.61±1.44
RESNET44- $\alpha_F$ p4m [17]	2.70	3.45	1.28	5.86±0.34
p4m-E4R18 [8]	6.0	3.87	0.65	4.96±0.16
ResNeXt29 [38]	6.81	1.08	0.16	4.36±0.25
ResNeXt29-FB-k3-WMCG-nb9 <sup>c</sup>	6.81	1.08	0.16	4.74±0.19
ResNeXt29-WT-k3-WMCG-nb9 <sup>d</sup>	6.81	1.08	0.16	4.07±0.15
ResNeXt29-WT-k3-WMCG-nb1-r2 <sup>c</sup>	4.74	1.08	0.23	<b>4.05±0.16</b>

Note: a) Here the RST-CNN refers to the model mnist\_ses\_rst\_vector\_56\_rot\_8\_interrot\_8 from [16].  
 b) "kn" means the filter size of hidden non- $1 \times 1$  convolutional layers is  $n \times n$ .  
 c) "nb n" means n bases used per filter. "nb1-m" means using only one Bessel basis with the (n + 1)-th lowest frequency (excluding the constant scalar basis).  
 d) The suffix "WT" means that the MH wavelet filter basis is used.

Table IV shows the accuracy results of STL10 under the ID and OOD settings. We find that SESN [12] achieves the highest accuracy under the ID setting but performs poorly under the OOD setting. Meanwhile, our WMCG-CNN achieves competitive ID accuracy and the highest OOD accuracy with fewer learnable parameters and lower computational complexity, which demonstrates the good generalization ability of our method.

#### D. Image classification experiments on ImageNet benchmark datasets

In this section, we test the proposed method on ImageNet1k datasets. In addition, we use ImageNet1k-C [47] validation datasets to test neural networks' robustness and generalizability against image corruptions, where 15 diverse corruption types [47] are included for both the ImageNet1k-C validation datasets. It should be noted that the ImageNet1k-C is not included in the training set but serves as out-of-distribution data to test the models' robustness and generalizability. Three

kinds of training routines are used: For tests with ResNets, we have robust training strategies (Pixmix) with affine transform augmentation included, and the corresponding controlled training routine without Pixmix augmentation; And the state-of-the-art full training strategy for tests with Swin [48] and ConvNeXt [49].

We use ResNeXt50 [38] as the baseline network for the Pixmix-based [40] robust training. We denote "ResNeXt50-k5-WMCG-nb9" as the network created by replacing the  $3 \times 3$  convolution layer with WMCG-CNN of the  $5 \times 5$  FB basis size and each convolutional filter using 9 bases. The neural networks are trained with the same strategy in Pixmix [40]. All the neural networks are trained from scratch to compare the sample efficiency and convergence speed of different networks.

In addition, we test our methods with the recently proposed ConvNeXt network model [49] on ImageNet40 and ImageNet1k datasets. We use ConvNeXt-S as the baseline network. We denote "ConvNeXt-S-k7-WMCG-nb49" as the network created by replacing all the  $7 \times 7$  convolution layer with WMCG-CNN of the  $7 \times 7$  FB basis size and each convolutional filter using 49 bases. The training on both datasets is in the same way as described in [49], where the neural networks are trained for 300 epochs using an AdamW optimizer. Similar to [49], the top 1 and top 5 accuracies are considered.

Although this paper focuses on equivariant CNNs, we note that the idea of "non-parameter-sharing" "weighted aggregation" is also adopted in other research works for image classification, such as dynamic convolutions [50]. Our methods differ from the dynamic convolutions in three aspects: 1) Dynamic convolutions generate weights via an attention module using a feature tensor as input, where the generated weights change with the changes in feature tensors. Our methods use learnable parameters directly as weights (these weights are learned only from the training phase), and the learned weights remain unchanged during the inference phase for different feature tensors; 2) Dynamic convolutions aggregate multiple learnable kernels, while our methods aggregate multiple augmented filters; 3) Dynamic convolutions focus on increasing the representation capability of neural networks by introducing an attention mechanism to aggregate multiple learnable kernels, and the number of learnable parameters is increased. Meanwhile, our methods focus on efficiently improving the affine equivariance of CNNs, without increasing computational complexity of inference; the number of learnable parameters is reduced or remains unchanged. To demonstrate the performance difference, we include the tests of dynamic convolutions in the following experiments.

Table V shows all the results for our image classification experiments. We see that with or without the robust training strategies (Pixmix), the proposed WMCG-CNNs reduce the classification errors on both clean and corrupted datasets while using the same or smaller number of parameters. It is also noted that a large filter size can help increase the classification precision and robustness of neural networks. The WMCG-CNN is good at exploiting large-size filters for boosting the performance. As for the experiment with ConvNeXt, WMCG-

TABLE IV

THE COMPARISON RESULTS OF IMAGE CLASSIFICATION EXPERIMENTS WITH PARAMETER-SHARING GROUP EQUIVARIANT NEURAL NETWORK MODELS ON STL10 DATASETS FOR BOTH IN-DISTRIBUTION (ID) AND OUT-OF-DISTRIBUTION (OOD) SETTINGS. THE TRAINING TIME (S/EPOCH), TRAINING VRAM FOOTPRINT (MB) AND INFERENCE TIME (S) ARE TESTED ON GPU NVIDIA A100 80GB.

	Params (M)	MACs (G)	MACs/Params (G/M)	Training Time (s/epoch)	Training VRAM Footprint (MB)	Inference Time (s)	ID Accuracy (%)	OOD Accuracy (%)
SESN [12]	10.96	227.02	28.47	89	30440	48	<b>91.22</b> ±0.24	82.30±0.41
RST-CNN [16]	9.74	850.23	106.62	437	79248	184	88.81±0.12	79.35±0.53
ResNeXt50 [38]	23.00	0.79	0.10	4	2354	3		
ResNeXt50-k7 <sup>a</sup>	8.15	10.05	1.26	27	21886	11	87.93±0.64	81.13±0.82
ResNeXt50-WMCG	7.97	10.05	1.28	31	23184	11	90.78±0.59	<b>83.71</b> ±0.45

Note: a) "kn" means the filter size of hidden non-1 × 1 convolutional layers is n × n.

CNN improves ConvNeXt-S on both ImageNet40 and ImageNet1k datasets without increasing the number of parameters and the computational burden. It is also noted that shear transform is also helpful for performance boost under the 300-epoch full-training routine. Dynamic convolution works well with a kernel size of 3 × 3, but performs poorly with a kernel size of 7 × 7. Furthermore, it performs poorly on the ImageNet1k-C dataset, which implies poor generalization ability.

TABLE V

THE RESULTS OF IMAGE CLASSIFICATION EXPERIMENTS WITH CNN MODELS ON MULTIPLE BENCHMARK DATASETS.

	Params (M)	MACs (G)	ImageNet1k Error (%)	ImageNet1k-C mCE (%)
<b>With Pixmix</b>				
ResNet50 [37]	25.56	4.12	25.78	54.23
ResNet50-DY <sup>a</sup>	59.83	4.19	<b>24.66</b>	55.34
ResNet50-k5-WMCG-nb9 <sup>b,c</sup>	25.56	7.41	25.26	<b>53.04</b>
ResNeXt50 [38]	25.03	4.27	23.27	51.16
ResNeXt50-DY	30.55	4.31	<b>22.00</b>	51.57
ResNeXt50-k5-WMCG-nb9	25.03	4.68	23.10	<b>50.57</b>
<b>Without Pixmix</b>				
ResNet50 [37]	25.56	4.12	23.52	61.52
ResNet50-DY	59.83	4.19	<b>23.24</b>	62.05
ResNet50-k5-WMCG-nb9	25.56	7.41	23.28	<b>61.12</b>
ResNeXt50 [38]	25.03	4.27	22.13	59.82
ResNeXt50-DY	30.55	4.31	22.09	60.36
ResNeXt50-k5-WMCG-nb9	25.03	4.68	<b>22.01</b>	<b>59.71</b>
<b>ImageNet40</b>				
	Params (M)	MACs (G)	Top-1 Acc. (%)	Top-5 Acc. (%)
ConvNeXt-S [49]	50.22	8.70	84.75	96.45
ConvNeXt-S-DY	53.70	8.71	<b>86.85</b>	94.50
ConvNeXt-S-k7-WMCG-nb49-shear0.00 <sup>d</sup>	50.22	8.70	85.85	<b>97.95</b>
ConvNeXt-S-k7-WMCG-nb49	50.22	8.70	86.65	97.80
<b>ImageNet1k</b>				
	Params (M)	MACs (G)	Top-1 Acc. (%)	Top-5 Acc. (%)
Swin-S [48]	49.61	8.75	83.17	96.23
ConvNeXt-S [49]	50.22	8.70	83.14	96.43
ConvNeXt-S-DY	53.70	8.71	82.57	96.17
ConvNeXt-S-k7-WMCG-nb49	50.22	8.70	<b>83.24</b>	<b>96.49</b>

Note: a) "DY" means the hidden non-1 × 1 CNN layers are replaced with a corresponding dynamic convolution [50] layer of the same kernel size.  
 b) "kn" means the filter size of hidden non-1 × 1 convolutional layers is n × n.  
 c) "nb n" means n bases used per filter.  
 d) "shear-n<sub>s</sub>π" denotes shear transform angle [-n<sub>s</sub>π, n<sub>s</sub>π]. n<sub>s</sub> = 0.00 means that there is no shear transform applied.

### E. Image denoising experiments on simulation and real noisy image sets

Although it has been shown that in certain cases with known noise levels, the traditional algorithms can surpass CNNs in denoising quality [51], [52], their processing speed is much slower than neural networks. Blind denoising with unknown noise levels is also a more practical scenario in the application. Thus in this paper, we only test the neural networks' performance on blind denoising tasks.

The experiments are divided into three parts: grayscale synthetic additive Gaussian noisy image denoising, color synthetic additive Gaussian noisy image denoising, and real-world color noisy image denoising (whose image noise is generated in the camera imaging process). For grayscale image denoising, as in [53], the same 400 180 × 180 images are used for

training. These images are cropped from each of the selected 400 images of the Berkeley segmentation dataset [4]. The Berkeley segmentation dataset includes 1,000 representative 481 × 321 RGB images from the Corel image database. The training images are corrupted by synthetic additive Gaussian noise of noise level (i.e., the standard deviation of noise)  $\sigma \in [0, 55]$ . 128 × 3,000 patches of size 50 × 50 are cropped to train the CNN model. For color synthetic noisy image denoising, we follow [54], where the same 400 color images are augmented with bicubic downscaling, counterclockwise rotation, and horizontal flip. As for real-world noisy images, as in [54], the training dataset consists of 100 512 × 512 JPEG images collected from five digital cameras Canon 80D, Nikon D800, Canon 600D, Sony A7 II and Canon 5D Mark II with an ISO of 800, 1,600, 3,200, 6,400, 12,800 and 25,600.

Five public test datasets are considered, including the grayscale image datasets Set12 [55], BSD68 [55], the color image datasets CBSD68 [55], Kodak24 [56], and the public real noisy consumer camera image dataset CC [57]. Set12 and BSD68 consist of 12 and 68 grayscale images derived from the Berkeley segmentation dataset [4], respectively. CBSD68 consists of 68 color images selected from the Berkeley segmentation dataset [4]. The Kodak24 dataset consists of 24 lossless, true color (24 bits per pixel) 768 × 512 images released by the Eastman Kodak Company. The public CC dataset consists of 15 images that are captured by three different digital cameras: Canon 5D Mark III, Nikon D600, and Nikon D800 with ISO values of 1,600, 3,200, or 6,400. The training images are cropped into 41 × 41 patches for training the networks.

We consider one of the most famous denoising CNNs, DnCNN-B [58] [53] as the baseline network for experiments on gray-scale image denoising. We build a brand new denoising network called DnNeXt-B by replacing every plain hidden CNN layer in DnCNN-B with the bottleneck block shown in Fig. 3(b). We further denote "DnNeXt-B-k5-WMCG-nb9" as the network created by replacing the hidden 3 × 3 convolution layer in DnNeXt-B with WMCG-CNN of the 5 × 5 FB basis size and each convolutional filter decomposed by 9 bases. Likewise, "DnNeXt-B-k7-WMCG-nb9" is a corresponding version with FB basis of size 7 × 7. To emphasize the efficiency of our approach, we also include another Wavelet-based denoising CNN, MWDCNN [59] for comparison. We test all the CNNs on the standard grayscale image datasets Set12 [55], and BSD68 [55]. The DnCNN, DnNeXt, and DnNeXt-WMCG are trained with the same training strategy as in [53]. We use SGD optimizer with a weight decay of 0.0001, and a momentum of 0.9. The networks are trained for

50 epochs with a batch size of 128. During the 50 epochs of training, the learning rate decreases exponentially from  $1.0 \times 10^{-1}$  to  $1.0 \times 10^{-4}$ .

Table VI shows the denoising results with the metric of peak signal-to-noise ratio (PSNR) on images corrupted by simulated white Gaussian noise of different noise levels. The number of trainable parameters and MACs are also displayed. In particular, for all the calculations of MACs in image-denoising experiments, we assume the input patch size is  $3 \times 32 \times 32$  for a fair comparison of computational burden, which differs from the actual case. We find that the proposed DnNeXt and DnNeXt-MCG outperform DnCNN and MWDCNN with a much smaller number of learnable parameters. In addition, the proposed DnNeXt-WMCG achieves the highest average PSNR of all CNNs and yields especially higher PSNR on high noise levels. The larger FB basis helps gain a higher PSNR score on high noise levels, yet may cause poor performance on low noise levels.

We consider DudeNet [54], an upgrading of DnCNN as the baseline CNN for the synthetic color noisy image denoising and real camera image denoising experiment. We build a new network DudeNeXt by replacing every plain hidden  $3 \times 3$  CNN layer in DudeNet with the bottleneck block shown in Fig. 3(b). We further denote "DudeNeXt-k5-WMCG-nb9" as the network created by replacing the hidden  $3 \times 3$  convolution layer in DudeNeXt with WMCG-CNN of the  $5 \times 5$  FB basis size and each convolutional filter decomposed by 9 bases. We follow the same training strategy as in [54]. We use Adam optimizer with an initial learning rate of  $1.0 \times 10^{-3}$  and a batch size of 128. The networks are trained for 70 epochs. During the 70 epochs of training, the learning rate decreases exponentially from  $1.0 \times 10^{-3}$  to  $1.0 \times 10^{-5}$ . On synthetic color noisy dataset, we compare our methods with two conventional denoising algorithms CBM3D [60], TID [61], as well as three deep learning methods DnCNN [53], DudeNet [54], and MWDCNN [59]. On the real noisy image set CC, we additionally include two transformer-inspired networks for comparison, i.e., Restormer [62] and NAFNet-width64 [63]. For a fair comparison, we keep using the same training set, batch size, and epoch number. For parameter stabilization, these two networks use their best optimizer setting, respectively. Specifically, as in [62], Restormer uses AdamW optimizer with an initial learning rate  $3e-4$ , betas (0.9, 0.999), weight decay  $1e-4$ , and cosine annealing learning rate scheduler. As in [63], NAFNet uses AdamW optimizer with an initial learning rate  $1e-3$ , betas (0.9, 0.9), weight decay 0, and cosine annealing learning rate scheduler.

Table VII shows the results on the public CBSD68 and Kodak24 color image datasets. Table VIII shows the results on the public CC dataset. The average PSNR, the parameter number, and MACs are displayed. Fig. 6 and Fig. 7 show the visual results on CC dataset. On both synthetic and real-world color image denoising experiments, the proposed networks achieve superior performance regarding the average PSNR. DudeNeXt-WMCG gives a competitive visual performance with a lightweight architecture. The performance of Restormer and NAFNet may be further improved with more advanced training and pretraining techniques as well as larger

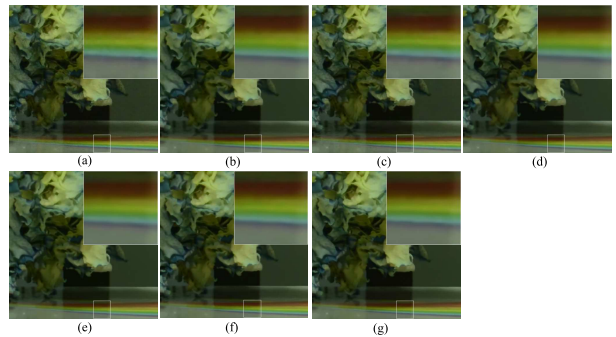


Fig. 6. Denoising results of a real noisy image by Nikon D800 ISO1600 from CC. (a) noisy image; (b) Dude; (c) MWDCNN; (d) Restormer; (e) NAFNet; (f) DudeNeXt; (g) DudeNeXt-B-k5-WMCG-nb9.

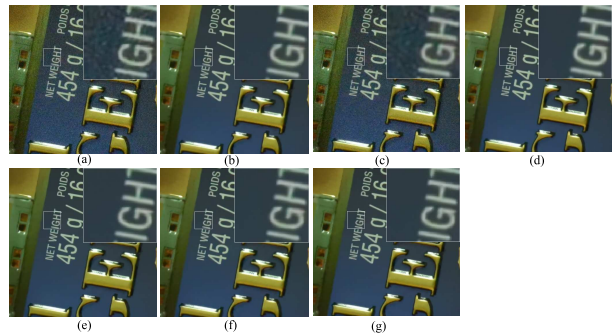


Fig. 7. Denoising results of a real noisy image by Nikon D800 ISO6400 from CC. (a) noisy image; (b) Dude; (c) MWDCNN; (d) Restormer; (e) NAFNet; (f) DudeNeXt; (g) DudeNeXt-B-k5-WMCG-nb9.

iteration number. Yet our focus is to test the methods' data efficiency and parameter efficiency. We see that the proposed method help achieve a lightweight denoising solution by improving the DudeNeXt's performance without increasing the computational burden, which uses far fewer parameter than transformer-inspired networks. In addition, regarding dynamic convolutions, they introduce more learnable parameters and exhibit inferior denoising performance compared to our methods. Similar to the results for image classification, dynamic convolutions work well with a kernel size of  $3 \times 3$  but perform poorly with a kernel size of  $5 \times 5$ .

## F. Analysis and discussion

The ablation experiments on ImageNet40 demonstrate the sample efficiency of WMCG-CNN for all the tested baseline network architectures including ResNet18, ResNet50, and ResNeXt50. We note that the proposed method gives a larger reduction in the Error for ResNet18 and ResNet50 than that for ResNeXt50. This is probably because a larger proportion of learnable parameters in ResNeXt50 lies in  $1 \times 1$  Conv layers which, as shown in the results, causes heavy overfitting on the small dataset ImageNet40.

The comparison experiments with discrete G-CNN, MCG-CNN, and WMCG-CNN on ImageNet prove that the diversity of transformations is helpful for a performance boost. Introducing MC sampling allows us to consider any mix of affine transforms. In the experiments on ImageNet40, we see that the

TABLE VI

THE AVERAGE PSNR (DB) OF DIFFERENT METHODS ON THE GRAYSACLE IMAGE DATASETS SET12 AND BSD68 WITH DIFFERENT NOISE LEVELS  $\sigma$  FROM 15 TO 50.

$\sigma$	Params (M)	MACs (G)	Set12				BSD68				Average
			15	25	35	50	15	25	35	50	
MWDCNN-B [59]	5.24	3.75	32.60	30.39	28.78	27.23	31.39	29.16	27.65	26.20	
DnCNN-B [53]	0.67	0.68	32.70	30.35	28.78	27.13	31.60	29.14	27.65	26.19	29.19
DnNet-B [54]	0.64	0.66	<b>32.76</b>	30.38	28.86	27.18	<b>31.65</b>	<b>29.18</b>	27.70	26.24	29.24
DnNet-B-k5-WMCG-nb9 <sup>a,b</sup>	0.64	1.26	32.74	<b>30.41</b>	28.89	27.30	31.56	29.16	27.72	26.31	<b>29.26</b>
DnNet-B-k7-WMCG-nb9	0.64	2.17	32.57	30.39	<b>28.96</b>	<b>27.37</b>	31.21	29.06	<b>27.74</b>	<b>26.33</b>	29.20

Note: a) "kn" means the filter size of hidden non-1  $\times$  1 convolutional layers is  $n \times n$ .  
 b) "nb n" means n bases used per filter.

TABLE VII

THE AVERAGE PSNR (DB) OF DIFFERENT METHODS ON THE COLOR IMAGE DATASETS CBSD68 AND KODAK24 WITH DIFFERENT NOISE LEVELS  $\sigma$  FROM 15 TO 50.

$\sigma$	Params (M)	MACs (G)	CBSD68				Kodak24				Average
			15	25	35	50	15	25	35	50	
CBM3D [60]			33.52	30.71	28.89	27.38	34.28	31.68	29.90	28.46	30.60
DnCNN [53]	0.56	0.57	33.98	31.31	29.65	28.01	34.73	32.23	30.64	29.02	31.20
FFDNet [64]	0.85	0.22	33.80	31.18	29.57	27.96	34.55	32.11	30.56	28.99	31.09
DudeNet [54]	1.08	1.11	34.01	31.34	29.71	28.09	34.81	32.26	30.69	29.10	31.25
MWDCNN [59]	5.25	3.76	34.18	31.45	29.81	28.13	34.91	32.40	30.87	29.26	31.38
MWDCNN-B [59]	5.25	3.76	34.10	31.44	29.80	28.15	34.83	32.39	30.83	29.23	31.35
DudeNet-B [54]	1.08	1.11	33.96	31.32	29.69	28.05	34.71	32.23	30.66	29.05	31.21
DudeNet-B	1.07	1.04	34.15	31.46	29.80	28.12	34.90	32.40	30.81	29.17	31.35
DudeNet-B-k5-WMCG-nb9 <sup>a,b</sup>	1.07	2.04	<b>34.19</b>	<b>31.53</b>	<b>29.90</b>	<b>28.27</b>	<b>34.96</b>	<b>32.49</b>	<b>30.94</b>	<b>29.35</b>	<b>31.45</b>

Note: a) "kn" means the filter size of hidden non-1  $\times$  1 convolutional layers is  $n \times n$ .  
 b) "nb n" means n basis used per filter.

TABLE VIII

THE PSNR (DB) OF DIFFERENT METHODS ON THE REAL-WORLD NOISY IMAGE DATASET CC [57] BY CUSTOMER CAMERAS.

Setting	Canon 5D ISO3200			Nikon D600 ISO3200			Nikon D800 ISO1600			Nikon D800 ISO3200			Nikon D800 ISO6400			Average	Params (M)	MACs (G)
CBM3D [60]	<b>39.76</b>	36.40	<b>36.37</b>	34.18	35.07	37.13	36.81	37.76	37.51	35.05	34.07	34.42	31.13	31.22	30.97	35.19		
TID [61]	37.22	34.54	34.25	32.99	34.20	35.58	34.49	35.19	35.26	33.70	31.04	33.07	29.40	29.86	29.21	33.36		
DnCNN [53]	37.26	34.13	34.09	33.62	34.48	35.41	37.95	36.08	35.48	34.08	33.70	33.31	29.83	30.55	30.09	33.86	0.56	0.57
DudeNet [54]	36.66	36.70	35.03	33.72	34.70	37.98	38.10	<b>39.15</b>	36.14	36.93	35.80	37.49	31.94	32.51	<b>32.91</b>	35.72	1.08	1.11
MWDCNN [59]	36.97	36.01	34.80	33.91	34.88	37.02	37.93	37.49	<b>38.44</b>	37.10	<b>36.72</b>	37.25	32.24	32.56	32.76	35.74	5.25	3.76
Restormer [62]	35.71	35.97	34.71	33.91	35.36	38.58	37.69	37.64	36.18	<b>37.96</b>	35.88	37.84	32.98	32.60	32.85	35.72	26.11	3.41
NAFNet [63]	35.99	36.96	35.16	32.81	35.01	<b>39.00</b>	37.29	38.65	36.93	38.34	36.33	<b>38.43</b>	32.31	32.67	32.22	35.87	115.98	1.01
DudeNet	36.69	36.45	35.00	33.67	34.52	37.78	38.20	38.51	37.07	37.24	36.29	37.80	32.32	32.19	32.55	35.75	1.07	1.04
DudeNet-k5 <sup>a</sup>	36.65	37.02	35.22	34.05	34.56	38.58	38.12	38.58	36.80	36.95	35.83	37.17	32.34	32.62	32.81	35.80	1.99	2.04
DudeNet-k3-DY <sup>b</sup>	36.00	36.82	35.40	33.65	<b>36.55</b>	37.74	38.10	38.20	36.14	37.71	36.51	38.27	31.94	<b>32.78</b>	32.91	35.91	2.77	1.10
DudeNet-k5-DY	36.49	34.01	33.62	33.86	34.33	35.36	35.18	35.22	34.66	33.43	32.62	32.89	29.76	30.13	30.05	33.44	6.57	2.07
DudeNet-k5-WMCG-nb9 <sup>c</sup>	36.91	<b>37.11</b>	35.15	<b>34.46</b>	35.64	38.89	<b>38.30</b>	38.81	37.30	37.72	35.99	37.76	<b>32.36</b>	32.77	32.90	<b>36.14</b>	1.07	2.04

Note: a) "kn" means the filter size of hidden non-1  $\times$  1 convolutional layers is  $n \times n$ .  
 b) "DY" means the hidden non-1  $\times$  1 CNN layers are replaced with a corresponding dynamic convolution [50] layer of the same kernel size.  
 c) "nb n" means n bases used per filter.

additional use of shear transform with a suitable shear range can consistently improve image classification. Meanwhile, a high degree of shear transform can harm the performance, which is because, in discrete implementation, shear transform leads to compression of information along a certain direction that causes information loss.

As we know a rotation transform can be decomposed into three shear transforms [65] as shown in equation (31), by combining one shear transform and one rotation transform, we can get all the possible rotation and shear transform (along horizontal or vertical direction), which thereby greatly increase the diversity of the considered transforms. In addition, shear transforms are common in daily life (as shown in Fig. 1). Obviously, a good machine learning model for classification and regression tasks usually should consider as many such kinds of group equivariance as possible.

$$R(\theta) = \begin{bmatrix} \cos \theta & \sin \theta \\ -\sin \theta & \cos \theta \end{bmatrix} = \begin{bmatrix} 1 & -\tan \frac{\theta}{2} \\ 0 & 1 \end{bmatrix} \cdot \begin{bmatrix} 1 & 0 \\ \sin \theta & 1 \end{bmatrix} \cdot \begin{bmatrix} 1 & -\tan \frac{\theta}{2} \\ 0 & 1 \end{bmatrix} \quad (31)$$

On the other hand, the shear-transform-augmented convolutional filters can be considered as an example of the classic continuous shear wavelet [34], [66]. The shear wavelet can help achieve a highly sparse representation of multidimensional data [66], which also explains the superior performance it brings to the proposed WMCG-CNN.

For the image denoising task, we did not manage to improve CNN's performance against Dirac delta basis on SIDD datasets [67]. There are two possible reasons: 1) The filter basis we are using is not optimal for SIDD datasets. 2) The noise level is very low on the SIDD dataset. The current non-Dirac-delta basis we are using works best with a larger kernel size, which, as shown in the experiments on simulation datasets, does not work well when the noise level is low. We may leave it to future work to find bases superior to the Dirac delta bases on SIDD datasets. Meanwhile, it is possible that we can combine the non-Dirac-delta basis with the Dirac-delta basis into a certain architecture to achieve superior performance. Since it is not the focus of this paper, we will not discuss it here.

We also note that in MC integral and stochastic simulation, there are a lot of advanced techniques such as quasi-MC

sampling [26], Markov chain MC [68], and multi-level MC [69]. There is a potential that these methods can help improve both MCG-CNN and WMCG-CNN further, and we will study this in future work.

The proposed WMCG-CNN shows higher flexibility and controllability than the conventional CNNs. The use of filter decomposition decouples the relationship between the filter size and the number of trainable parameters. For a certain convolutional kernel, the corresponding number of trainable parameters can be as small as only 1, or as large as any integer. In addition, we can choose a certain custom design basis as one likes to control the performance of the network. For example, in the experiment on the CIFAR10 dataset, we simply choose a single low-frequency wavelet basis and can still get a good result on the CIFAR10 dataset. It is noted that the choice of filter basis can greatly affect the performance of WMCG-CNN. For different datasets, the optimal basis type and basis size can be different.

#### IV. CONCLUSION

In this paper, we propose an efficient and flexible implementation of group-equivariant CNN based on filter-wise weighted Monte Carlo sampling, which allows a higher degree of diversity of transformations for a performance boost. Compared with parameter-sharing G-CNN, with a suitable filter basis, the proposed non-parameter-sharing WMCG-CNN can exploit deeper neural network architectures without causing heavy computational burden and achieves superior performance. The proposed WMCG-CNN is shown to be an efficient generalization of standard CNN. The utility of diverse transformations for tasks on natural images is demonstrated. The proposed WMCG-CNN shows superior efficiency on both image classification and image denoising tasks when using a suitable set of filter bases. It is possible to extend it for other computer vision tasks such as image segmentation and image reconstruction. However, the choice of filter basis is a key point for yielding good performance with the proposed method, which will be studied in future work.

#### ACKNOWLEDGMENTS

This work was supported by the Deutsche Forschungsgemeinschaft (DFG) under grant no. 428149221, by Deutsches Zentrum für Luft- und Raumfahrt e.V. (DLR), Germany under grant no. 01ZZ2105A and no. 01KD2214, and by Fraunhofer Gesellschaft e.V. under grant no. 017-100240/B7-aneg. The authors would like to thank Ulrike Attenberger for her contribution to funding acquisition.

#### REFERENCES

- [1] R. Wang, R. Walters, and R. Yu, "Data augmentation vs. equivariant networks: A theory of generalization on dynamics forecasting," *arXiv preprint arXiv:2206.09450*, 2022.
- [2] F. Quiroga, F. Ronchetti, L. Lanzarini, and A. F. Bariviera, "Revisiting data augmentation for rotational invariance in convolutional neural networks," in *Modelling and Simulation in Management Sciences: Proceedings of the International Conference on Modelling and Simulation in Management Sciences (MS-18)*. Springer, 2020, pp. 127–141.
- [3] R. Kondor and S. Trivedi, "On the generalization of equivariance and convolution in neural networks to the action of compact groups," in *International Conference on Machine Learning*. PMLR, 2018, pp. 2747–2755.
- [4] D. Martin, C. Fowlkes, D. Tal, and J. Malik, "A database of human segmented natural images and its application to evaluating segmentation algorithms and measuring ecological statistics," in *Proceedings eighth IEEE international conference on computer vision. ICCV 2001*, vol. 2. IEEE, 2001, pp. 416–423.
- [5] K. Fukushima, "Neocognitron: A self-organizing neural network model for a mechanism of pattern recognition unaffected by shift in position," *Biological cybernetics*, vol. 36, no. 4, pp. 193–202, 1980.
- [6] Y. LeCun, B. Boser, J. S. Denker, D. Henderson, R. E. Howard, W. Hubbard, and L. D. Jackel, "Backpropagation applied to handwritten zip code recognition," *Neural computation*, vol. 1, no. 4, pp. 541–551, 1989.
- [7] P. Krüger and H. Gottschalk, "Equivariant and steerable neural networks: A review with special emphasis on the symmetric group," *arXiv preprint arXiv:2301.03019*, 2023.
- [8] L. He, Y. Chen, Y. Dong, Y. Wang, Z. Lin *et al.*, "Efficient equivariant network," *Advances in Neural Information Processing Systems*, vol. 34, pp. 5290–5302, 2021.
- [9] C. Lyle, M. Kwiatkowska, and Y. Gal, "An analysis of the effect of invariance on generalization in neural networks," in *International conference on machine learning Workshop on Understanding and Improving Generalization in Deep Learning*, vol. 1, 2019.
- [10] T. Cohen and M. Welling, "Group equivariant convolutional networks," in *International conference on machine learning*. PMLR, 2016, pp. 2990–2999.
- [11] T. S. Cohen and M. Welling, "Steerable cnns," *arXiv preprint arXiv:1612.08498*, 2016.
- [12] I. Sosnovik, M. Szmaja, and A. Smeulders, "Scale-equivariant steerable networks," *arXiv preprint arXiv:1910.11093*, 2019.
- [13] I. Sosnovik, A. Moskalev, and A. Smeulders, "Disco: accurate discrete scale convolutions," *arXiv preprint arXiv:2106.02733*, 2021.
- [14] M. Sangalli, S. Blusseau, S. Velasco-Forero, and J. Angulo, "Scale equivariant neural networks with morphological scale-spaces," in *Discrete Geometry and Mathematical Morphology: First International Joint Conference, DGMM 2021, Uppsala, Sweden, May 24–27, 2021, Proceedings*. Springer, 2021, pp. 483–495.
- [15] W. Zhu, Q. Qiu, R. Calderbank, G. Sapiro, and X. Cheng, "Scaling-translation-equivariant networks with decomposed convolutional filters," *Journal of machine learning research*, vol. 23, no. 68, pp. 1–45, 2022.
- [16] L. Gao, G. Lin, and W. Zhu, "Deformation robust roto-scale-translation equivariant cnns," *arXiv preprint arXiv:2111.10978*, 2021.
- [17] D. Romero, E. Bekkers, J. Tomczak, and M. Hoogendoorn, "Attentive group equivariant convolutional networks," in *International Conference on Machine Learning*. PMLR, 2020, pp. 8188–8199.
- [18] Z. Sun and T. Blu, "Empowering networks with scale and rotation equivariance using a similarity convolution," in *The Eleventh International Conference on Learning Representations*, 2023. [Online]. Available: <https://openreview.net/forum?id=NJENSJ37sQ>
- [19] T. S. Cohen, M. Geiger, and M. Weiler, "A general theory of equivariant cnns on homogeneous spaces," *Advances in neural information processing systems*, vol. 32, 2019.
- [20] Z. Yang, Y. Yu, C. You, J. Steinhardt, and Y. Ma, "Rethinking bias-variance trade-off for generalization of neural networks," in *International Conference on Machine Learning*. PMLR, 2020, pp. 10 767–10 777.
- [21] P. Nakkiran, G. Kaplun, Y. Bansal, T. Yang, B. Barak, and I. Sutskever, "Deep double descent: Where bigger models and more data hurt," *Journal of Statistical Mechanics: Theory and Experiment*, vol. 2021, no. 12, p. 124003, 2021.
- [22] D. S. Dummit, R. M. Foote *et al.*, *Abstract algebra*. Wiley Hoboken, 2004, vol. 3.
- [23] E. J. Bekkers, "B-spline cnns on lie groups," *arXiv preprint arXiv:1909.12057*, 2019.
- [24] K. Atkinson, *An introduction to numerical analysis*. John wiley & sons, 1991.
- [25] S. Weinzierl, "Introduction to monte carlo methods," *arXiv preprint hep-ph/0006269*, 2000.
- [26] R. E. Caflisch, "Monte carlo and quasi-monte carlo methods," *Acta numerica*, vol. 7, pp. 1–49, 1998.
- [27] G. P. Lepage, "A new algorithm for adaptive multidimensional integration," *Journal of Computational Physics*, vol. 27, no. 2, pp. 192–203, 1978.

- [28] P. Przybyłowicz, “Foundations of monte carlo methods and stochastic simulations—from monte carlo lebesgue integration to weak approximation of sdes,” *arXiv preprint arXiv:2208.05531*, 2022.
- [29] A. Kong, P. McCullagh, X.-L. Meng, D. Nicolae, and Z. Tan, “A theory of statistical models for monte carlo integration,” *Journal of the Royal Statistical Society: Series B (Statistical Methodology)*, vol. 65, no. 3, pp. 585–604, 2003.
- [30] T. Kiria and G. Pantsulaia, “Calculation of lebesgue integrals by using uniformly distributed sequences,” *Transactions of A. Razmadze Mathematical Institute*, vol. 170, no. 3, pp. 402–409, 2016.
- [31] P. W. Glynn and D. L. Iglehart, “Importance sampling for stochastic simulations,” *Management science*, vol. 35, no. 11, pp. 1367–1392, 1989.
- [32] Q. Qiu, X. Cheng, G. Sapiro *et al.*, “Dcnnet: Deep neural network with decomposed convolutional filters,” in *International Conference on Machine Learning*. PMLR, 2018, pp. 4198–4207.
- [33] H. Ryan, “Ricker, ormsby; klander, bntterwo-a choice of wavelets,” 1994.
- [34] J.-P. Antoine, P. Carrette, R. Murenzi, and B. Piette, “Image analysis with two-dimensional continuous wavelet transform,” *Signal processing*, vol. 31, no. 3, pp. 241–272, 1993.
- [35] Y. Wang, “Frequencies of the ricker wavelet,” *Geophysics*, vol. 80, no. 2, pp. A31–A37, 2015.
- [36] T. C. Hesterberg, “What teachers should know about the bootstrap: Resampling in the undergraduate statistics curriculum,” *The american statistician*, vol. 69, no. 4, pp. 371–386, 2015.
- [37] K. He, X. Zhang, S. Ren, and J. Sun, “Deep residual learning for image recognition,” in *Proceedings of the IEEE conference on computer vision and pattern recognition*, 2016, pp. 770–778.
- [38] S. Xie, R. Girshick, P. Dollár, Z. Tu, and K. He, “Aggregated residual transformations for deep neural networks,” in *Proceedings of the IEEE conference on computer vision and pattern recognition*, 2017, pp. 1492–1500.
- [39] D. Worrall and M. Welling, “Deep scale-spaces: Equivariance over scale,” *Advances in Neural Information Processing Systems*, vol. 32, 2019.
- [40] D. Hendrycks, A. Zou, M. Mazeika, L. Tang, B. Li, D. Song, and J. Steinhardt, “Pixmix: Dreamlike pictures comprehensively improve safety measures,” in *Proceedings of the IEEE/CVF Conference on Computer Vision and Pattern Recognition*, 2022, pp. 16783–16792.
- [41] A. Coates, A. Ng, and H. Lee, “An analysis of single-layer networks in unsupervised feature learning,” in *Proceedings of the fourteenth international conference on artificial intelligence and statistics*. JMLR Workshop and Conference Proceedings, 2011, pp. 215–223.
- [42] A. Krizhevsky, G. Hinton *et al.*, “Learning multiple layers of features from tiny images,” 2009.
- [43] Y. LeCun, L. Bottou, Y. Bengio, and P. Haffner, “Gradient-based learning applied to document recognition,” *Proceedings of the IEEE*, vol. 86, no. 11, pp. 2278–2324, 1998.
- [44] D. Marcos, B. Kellenberger, S. Lobry, and D. Tuia, “Scale equivariance in cnns with vector fields,” *arXiv preprint arXiv:1807.11783*, 2018.
- [45] R. Ghosh and A. K. Gupta, “Scale steerable filters for locally scale-invariant convolutional neural networks,” *arXiv preprint arXiv:1906.03861*, 2019.
- [46] D. Hendrycks, N. Mu, E. D. Cubuk, B. Zoph, J. Gilmer, and B. Laksminarayanan, “Augmix: A simple data processing method to improve robustness and uncertainty,” *arXiv preprint arXiv:1912.02781*, 2019.
- [47] D. Hendrycks and T. Dietterich, “Benchmarking neural network robustness to common corruptions and perturbations,” *arXiv preprint arXiv:1903.12261*, 2019.
- [48] Z. Liu, Y. Lin, Y. Cao, H. Hu, Y. Wei, Z. Zhang, S. Lin, and B. Guo, “Swin transformer: Hierarchical vision transformer using shifted windows,” in *Proceedings of the IEEE/CVF international conference on computer vision*, 2021, pp. 10012–10022.
- [49] Z. Liu, H. Mao, C.-Y. Wu, C. Feichtenhofer, T. Darrell, and S. Xie, “A convnet for the 2020s,” in *Proceedings of the IEEE/CVF Conference on Computer Vision and Pattern Recognition*, 2022, pp. 11976–11986.
- [50] Y. Chen, X. Dai, M. Liu, D. Chen, L. Yuan, and Z. Liu, “Dynamic convolution: Attention over convolution kernels,” in *Proceedings of the IEEE/CVF conference on computer vision and pattern recognition*, 2020, pp. 11030–11039.
- [51] W. Zhao, Y. Lv, Q. Liu, and B. Qin, “Detail-preserving image denoising via adaptive clustering and progressive pca thresholding,” *IEEE Access*, vol. 6, pp. 6303–6315, 2018.
- [52] W. Zhao, Q. Liu, Y. Lv, and B. Qin, “Texture variation adaptive image denoising with nonlocal pca,” *IEEE Transactions on Image Processing*, vol. 28, no. 11, pp. 5537–5551, 2019.
- [53] K. Zhang, W. Zuo, Y. Chen, D. Meng, and L. Zhang, “Beyond a gaussian denoiser: Residual learning of deep cnn for image denoising,” *IEEE transactions on image processing*, vol. 26, no. 7, pp. 3142–3155, 2017.
- [54] C. Tian, Y. Xu, W. Zuo, B. Du, C.-W. Lin, and D. Zhang, “Designing and training of a dual cnn for image denoising,” *Knowledge-Based Systems*, vol. 226, p. 106949, 2021.
- [55] H. Li, J. Cai, T. N. A. Nguyen, and J. Zheng, “A benchmark for semantic image segmentation,” in *2013 IEEE International Conference on Multimedia and Expo (ICME)*. IEEE, 2013, pp. 1–6.
- [56] R. Franzen, “Kodak lossless true color image suite,” source: <http://r0k.us/graphics/kodak>, vol. 4, no. 2, 1999.
- [57] S. Nam, Y. Hwang, Y. Matsushita, and S. J. Kim, “A holistic approach to cross-channel image noise modeling and its application to image denoising,” in *Proceedings of the IEEE conference on computer vision and pattern recognition*, 2016, pp. 1683–1691.
- [58] H. C. Burger, C. J. Schuler, and S. Harmeling, “Image denoising: Can plain neural networks compete with bm3d?” in *2012 IEEE Conference on Computer Vision and Pattern Recognition*, 2012, pp. 2392–2399.
- [59] C. Tian, M. Zheng, W. Zuo, B. Zhang, Y. Zhang, and D. Zhang, “Multi-stage image denoising with the wavelet transform,” *Pattern Recognition*, vol. 134, p. 109050, 2023.
- [60] K. Dabov, A. Foi, V. Katkovnik, and K. Egiazarian, “Image denoising by sparse 3-d transform-domain collaborative filtering,” *IEEE Transactions on image processing*, vol. 16, no. 8, pp. 2080–2095, 2007.
- [61] E. Luo, S. H. Chan, and T. Q. Nguyen, “Adaptive image denoising by targeted databases,” *IEEE transactions on image processing*, vol. 24, no. 7, pp. 2167–2181, 2015.
- [62] S. W. Zamir, A. Arora, S. Khan, M. Hayat, F. S. Khan, and M.-H. Yang, “Restormer: Efficient transformer for high-resolution image restoration,” in *Proceedings of the IEEE/CVF conference on computer vision and pattern recognition*, 2022, pp. 5728–5739.
- [63] L. Chen, X. Chu, X. Zhang, and J. Sun, “Simple baselines for image restoration,” in *European Conference on Computer Vision*. Springer, 2022, pp. 17–33.
- [64] K. Zhang, W. Zuo, and L. Zhang, “Ffdnet: Toward a fast and flexible solution for cnn-based image denoising,” *IEEE Transactions on Image Processing*, vol. 27, no. 9, pp. 4608–4622, 2018.
- [65] E. Andres, “The quasi-shear rotation,” in *Discrete Geometry for Computer Imagery: 6th International Workshop, DGCI’96 Lyon, France, November 13–15, 1996 Proceedings 6*. Springer, 1996, pp. 307–314.
- [66] K. Guo, G. Kutyniok, and D. Labate, “Sparse multidimensional representations using anisotropic dilation and shear operators,” 2006.
- [67] A. Abdelhamed, S. Lin, and M. S. Brown, “A high-quality denoising dataset for smartphone cameras,” in *Proceedings of the IEEE conference on computer vision and pattern recognition*, 2018, pp. 1692–1700.
- [68] M. K. Cowles and B. P. Carlin, “Markov chain monte carlo convergence diagnostics: a comparative review,” *Journal of the American Statistical Association*, vol. 91, no. 434, pp. 883–904, 1996.
- [69] M. B. Giles, “Multilevel monte carlo methods,” *Acta numerica*, vol. 24, pp. 259–328, 2015.